

---

# No Representation Rules Them All in Category Discovery

---

Anonymous Author(s)

Affiliation

Address

email

## Abstract

1 In this paper we tackle the problem of Generalized Category Discovery (GCD).  
2 Given a dataset with labelled and unlabelled images, the task is to cluster all images  
3 in the unlabelled subset, whether or not they belong to the labelled categories. Our  
4 first contribution is to recognize that most existing GCD benchmarks only contain  
5 labels for a single clustering of the data, making it difficult to ascertain whether  
6 models are using the available labels to solve the GCD task, or simply solving an  
7 unsupervised clustering problem. As such, we present a synthetic dataset, named  
8 ‘Clevr-4’, for category discovery. Clevr-4 contains four equally valid partitions  
9 of the data, *i.e.* based on object *shape*, *texture*, *color* or *count*. To solve the task,  
10 models are required to extrapolate the taxonomy specified by the labelled set, rather  
11 than simply latching onto a single natural grouping of the data. We use this dataset  
12 to demonstrate the limitations of unsupervised clustering in the GCD setting;  
13 showing that even very strong unsupervised models fail on Clevr-4, and further  
14 reveal that they each have characteristic biases from their pre-training. We also  
15 use Clevr-4 to examine the weaknesses of existing GCD algorithms, and propose a  
16 new method which addresses these shortcomings, outperforming state-of-the-art  
17 models on Clevr-4 and the challenging Semantic Shift Benchmark.

18 

## 1 Introduction

19 Developing algorithms which can classify images within complex visual taxonomies, *i.e.* image  
20 recognition, remains a fundamental task in machine learning [1–3]. However, most models require  
21 these taxonomies to be *pre-defined* and *fully specified*, and are unable to construct them automatically  
22 from data. The ability to *build* a taxonomy is not only desirable in many applications, but is also  
23 considered a core aspect of human cognition [4–6]. The task of constructing a taxonomy is epitomized  
24 by the Generalized Category Discovery (GCD) problem [7, 8]: given a dataset of images which is  
25 labelled only in part, the goal is to label all remaining images, using categories that occur in the  
26 labelled subset, or by identifying new ones. For instance, in a supermarket, given only labels for  
27 ‘spaghetti’ and ‘penne’ pasta products, a model must understand the concept of ‘pasta shape’ well  
28 enough to generalize to ‘macaroni’ and ‘fusilli’. It must *not* cluster new images based on, for instance,  
29 the color of the packaging, even though the latter *also* yields a valid, but different, taxonomy.

30 GCD is related to self-supervised learning [9] and unsupervised clustering [10], which can discover  
31 *some* meaningful taxonomies automatically [11]. However, these *cannot* solve the GCD problem,  
32 which requires recovering *any* of the different and incompatible taxonomies that apply to the same  
33 data. Instead, the key to GCD is in *extrapolating a taxonomy* which is only partially known. In this  
34 paper, our objective is to better understand the GCD problem and improve algorithms’ performance.

35 To this end, in section 2, we introduce the Clevr-4 dataset. Clevr-4 is a synthetic dataset where  
36 each image is fully parameterized by a set of four attributes, and where each attribute defines an  
37 equally valid grouping of the data (see fig. 1). Clevr-4 extends the original CLEVR dataset [12] by  
38 introducing new *shapes*, *colors* and *textures*, as well as allowing different object *counts* to be present  
39 in the image. Using these four attributes, the same set of images can be clustered according to *four*  
40 statistically independent taxonomies. This feature sets it apart from most existing GCD benchmarks,  
41 which only contain sufficient annotations to evaluate a *single* clustering of the data.

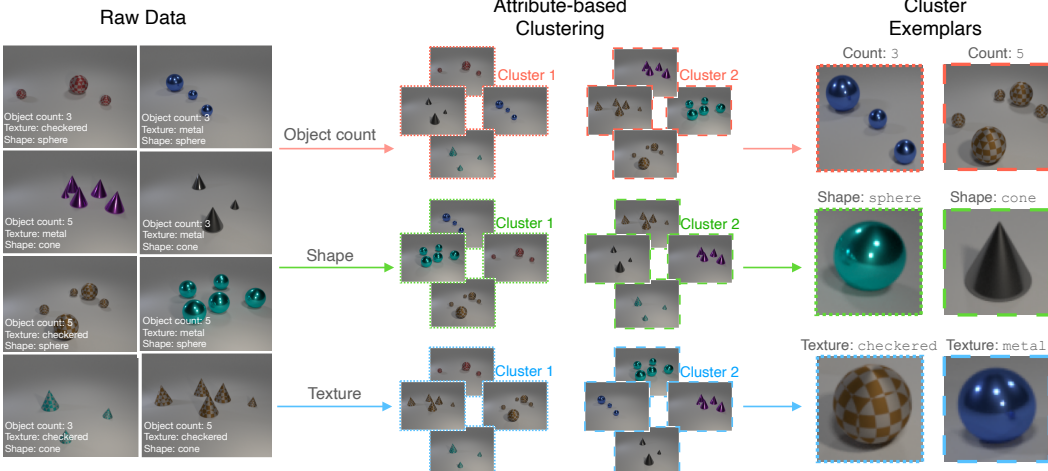


Figure 1: What is the key difference between Generalized Category Discovery (GCD) and tasks like self-supervised learning or unsupervised clustering? GCD’s key challenge is extrapolating the *desired* clustering of data given only a subset of possible category labels. We present a synthetic dataset, Clevr-4, which contains *four* possible clusterings of the same images, and hence can be used to isolate the GCD task. Above, one can cluster the data based on *object count*, *shape* or *texture*.

42 Clevr-4 allows us to probe large pre-trained models for biases, *i.e.*, for their preference to emphasize  
 43 a particular aspect of images, such as color or texture, which influences which taxonomy can be  
 44 learned. For instance, contrary to findings from Geirhos *et al.* [13], we find almost every large model  
 45 exhibits a strong shape bias. Specifically, in section 3, we find unsupervised clustering – even with  
 46 very strong representations like DINO [14] and CLIP [15] – fails on many splits of Clevr-4, despite  
 47 CLEVR being considered a ‘toy’ problem in other contexts [16]. As a result, we find that different  
 48 pre-trained models yield different performance traits across Clevr-4 when used as initialization for  
 49 category discovery. We further use Clevr-4 to characterize the weaknesses of existing category  
 50 discovery methods; namely, the harms of jointly training feature-space and classifier losses, as well  
 51 as insufficiently robust pseudo-labelling strategies for ‘New’ classes.

52 We make the following key contributions: **(i)** We propose a new benchmark dataset, Clevr-4, for GCD  
 53 and related tasks. Clevr-4 contains four independent taxonomies and can be used to precisely study the  
 54 category discovery problem. **(ii)** We use Clevr-4 to garner insights on the biases of large pre-trained  
 55 models as well as the weaknesses of existing category discovery methods. We demonstrate that  
 56 even very strong unsupervised models fail on this ‘toy’ benchmark. Furthermore, in appendix A, we  
 57 leverage our findings to develop a simple but performant method for GCD. Our method, inspired by  
 58 ‘mean-teachers’ and termed ‘ $\mu$ GCD’ (‘mean-GCD’), substantially outperforms current state-of-the-art,  
 59 both on the introduced Clevr-4 and on the challenging Semantic Shift Benchmark [17].

## 60 2 Clevr-4: a synthetic dataset for generalized category discovery

61 **The category discovery challenge.** Generalized Category Discovery (GCD) is the task of, given  
 62 a dataset with some labelled images and some unlabelled images, classifying all images in the  
 63 unlabelled subset. Here, unlabelled images may come from the labelled (‘Old’) categories or from  
 64 ‘New’ ones. As such, the key to category discovery (generalized or not) is to use the labelled  
 65 subset of the data to *extrapolate a taxonomy* and discover novel categories in unlabelled images.  
 66 This task of extrapolating a taxonomy sets category discovery apart from related problems. For  
 67 instance, unsupervised clustering [10] aims to find the single most natural grouping of unlabelled  
 68 images given only weak inductive biases (*e.g.*, invariance to specific data augmentations), but permits  
 69 limited control on *which* taxonomy is discovered. Meanwhile, semi-supervised learning [18] assumes  
 70 supervision for all categories in the taxonomy, which therefore must be known, in full, a-priori.

71 A problem with many current benchmarks for category discovery is that there is no clear taxonomy  
 72 underlying the object categories (*e.g.*, CIFAR [19]) and, when there is, it is often ill-posed to  
 73 understand it given only a few classes (*e.g.*, ImageNet-100 [20]). Furthermore, in practical scenarios,  
 74 there are likely to be many taxonomies of interest. However, few datasets contain sufficiently  
 75 complete annotations to evaluate multiple possible groupings of the same data. This makes it difficult  
 76 to ascertain whether a model is extrapolating information from the labelled set (category discovery)  
 77 or just finding its own most natural grouping of the unlabelled data (unsupervised clustering).

Table 2: **Unsupervised clustering accuracy (ACC) of pre-trained models on Clevr-4.** We find most models are strongly biased towards *shape*, while MAE [26] exhibits a *color* bias.

Pre-training Method	Pre-training Data	Backbone	Texture	Shape	Color	Count	Average
SWaV [9]	ImageNet-1K	ResNet50	13.1	65.5	12.1	<b>18.9</b>	27.4
MoCoV2 [27]	ImageNet-1K	ResNet50	13.0	77.5	12.3	18.8	30.4
Supervised [2]	ImageNet-1K	ResNet50	13.2	76.8	15.2	12.9	29.5
DINO [14]	ImageNet-1K	ViT-B/16	<b>16.0</b>	86.2	11.5	13.0	31.7
MAE [26]	ImageNet-1K	ViT-B/16	15.1	13.5	<b>64.7</b>	13.9	26.8
iBOT [28]	ImageNet-1K	ViT-B/16	14.4	85.9	11.5	13.0	31.2
CLIP [15]	WIP-400M	ViT-B/16	12.4	78.7	12.3	17.9	30.3
DINOv2 [29]	LVD-142M	ViT-B/14	11.6	<b>98.1</b>	11.6	12.8	<b>33.5</b>

- 78 **Clevr-4.** In order to better study this problem,  
 79 we introduce Clevr-4, a synthetic  
 80 benchmark which contains four equally  
 81 valid groupings of the data. Clevr-4  
 82 extends the CLEVR dataset [12], using  
 83 Blender [21] to render images of multiple  
 84 objects and place them in a static scene.  
 85 This is well suited for category discovery,  
 86 as each object attribute defines a different  
 87 taxonomy for the data (*e.g.*, it enables clustering images based on object *shape*, *color* etc.). The  
 88 original dataset is limited as it contains only three shapes and two textures, reducing the difficulty of  
 89 the respective clustering tasks. We introduce 2 new colors, 7 new shapes and 8 new textures to the  
 90 dataset, placing between 1 and 10 objects in each scene.
- 91 Each image is therefore parameterized by object *shape*, *texture*, *color* and *count*. The value for each  
 92 attribute is sampled uniformly and independently from the others, meaning the image label with  
 93 respect to one taxonomy gives us no information about the label with respect to another. Note that this  
 94 sets Clevr-4 apart from existing GCD benchmarks such as CIFAR-100 [19] and FGVC-Aircraft [22].  
 95 These datasets only contain taxonomies at different *granularities*, and as such the taxonomies are  
 96 highly correlated with each other. Furthermore, the number of categories provides no information  
 97 regarding the specified taxonomy, as all Clevr-4 taxonomies contain  $k = 10$  object categories.
- 98 Finally, we create GCD splits for each taxonomy in Clevr-4, following standard practise and reserving  
 99 half the categories for the labelled set, and half for the unlabelled set. We further subsample 50% of  
 100 the images from the labelled categories and add them to the unlabelled set. The dataset is procedurally  
 101 generated, and we synthesize 8.4K images for training. The full summary statistics of each split is  
 102 given in table 1, and the full generation procedure is detailed in the supplementary.

### 103 3 Learnings from Clevr-4 for category discovery

- 104 **Unsupervised clustering of pre-trained representations (table 2).** We first demonstrate the limita-  
 105 tions of unsupervised clustering of features as an approach for category discovery (reporting results  
 106 with semi-supervised clustering in fig. 10). Specifically, we run  $k$ -means clustering [23] on top of  
 107 features extracted with self- [9, 14, 24], weakly- [15], and fully-supervised [2, 3, 25] backbones,  
 108 reporting performance on each of the four taxonomies in Clevr-4. The representations are trained on  
 109 up to 400M images and are commonly used in the vision literature.
- 110 We find that most models perform well on the *shape* taxonomy, with DINOv2 achieving over 98%  
 111 accuracy. However, no model performs well across the board. For instance, on some splits (*e.g.*,  
 112 *color*), strong models like DINOv2 perform comparably to random chance. This underscores the  
 113 utility of Clevr-4 for delineating category discovery from standard representation learning. Logically,  
 114 it is *impossible* for unsupervised clustering on *any* representation to perform well on all tasks. After  
 115 all, only a single clustering of the data is produced, which cannot align with more than one taxonomy.  
 116 We highlight that such limitations are *not* revealed by existing benchmarks; on the CUB dataset,  
 117 unsupervised clustering with DINOv2 achieves 68% ACC ( $\approx 140 \times$  random, see table 5).

- 118 **Pre-trained representations for category discovery (table 3).** Many category discovery methods  
 119 use self-supervised representation learning for initialization in order to leverage large-scale pre-  
 120 training, in the hope of improving downstream performance. However, as shown above, these

Table 3: **Effects of large-scale pre-training on category discovery accuracy (ACC) on Clevr-4.**  
We find that large-scale pre-training provides inconsistent gains on Clevr-4.

Method	Backbone	Pre-training (Data)	Texture	Shape	Color	Count	Average	Average Rank
SimGCD	ResNet18	-	58.1	97.8	96.7	<b>67.6</b>	<b>80.5</b>	<b>2.0</b>
SimGCD	ViT-B/16	MAE [26] (ImageNet-1k)	54.1	99.7	<b>99.9</b>	53.0	76.7	<b>2.0</b>
SimGCD	ViT-B/14	DINOv2 [29] (LVD-142M)	<b>76.5</b>	<b>99.9</b>	87.4	51.3	78.8	<b>2.0</b>

Table 4: **Category discovery accuracy (ACC) on Clevr-4.** We find a much reduced gap between the GCD baseline [7] and SimGCD state-of-the-art [30], and further find our proposed  $\mu$ GCD provides substantial boosts (see supplementary). Results are averages across five random seeds.

Model	Backbone	Texture			Shape			Color			Count			Average
		All	Old	New	All	Old	New	All	Old	New	All	Old	New	
		All	Old	New	All	Old	New	All	Old	New	All	Old	New	
Fully supervised	ResNet18	99.1	-	-	100.0	-	-	100.0	-	-	96.8	-	-	99.0
GCD	ResNet18	62.4	97.5	45.3	93.9	99.7	90.5	90.7	95.0	88.5	71.9	96.4	60.1	79.7
SimGCD	ResNet18	58.1	95.0	40.2	<b>97.8</b>	98.9	<b>97.2</b>	96.7	99.9	95.1	67.6	95.7	53.9	80.1
$\mu$ GCD (Ours)	ResNet18	<b>69.8</b>	<b>99.0</b>	<b>55.5</b>	94.9	<b>99.7</b>	92.1	<b>99.5</b>	<b>100.0</b>	<b>99.2</b>	<b>75.5</b>	<b>96.6</b>	<b>65.2</b>	<b>84.9</b>

representations are biased. Here, we investigate the impact of these biases on a state-of-the-art method in generalized category discovery, SimGCD [30]. SimGCD contains two main loss components: (1) a contrastive loss on backbone features, using self-supervised InfoNCE [31] on all data, and supervised contrastive learning [32] on images with labels available; and (2) a contrastive loss to train a classification head, where different views of the same image provide pseudo-labels for each other. For comparison, we initialize SimGCD with a lightweight ResNet18 trained scratch; a ViT-B/16 pre-trained with masked auto-encoding [26]; and a ViT-B/14 with DINOv2 [29] initialization.

Surprisingly, and in stark contrast to most of the computer vision literature, we find inconsistent gains from leveraging large-scale pre-training on Clevr-4. For instance, on the *count* taxonomy, pre-training gives substantially *worse* performance than training a lightweight ResNet18 from scratch. On average across all splits, SimGCD with a randomly initialized ResNet18 actually performs best. Generally, we find that the final category discovery model inherits biases built into the pre-training, and can struggle to overcome them even after finetuning. Our results highlight the importance of carefully selecting the initialization for a given GCD task, and point to the utility of Clevr-4 for doing so.

**Limitations of existing category discovery methods.** Next, we analyze SimGCD [30], the current state-of-the-art for the GCD task. We show that on Clevr-4 it is not always better than the GCD baseline [7] which it extends, and identify the source of this issue in the generation of the pseudo-labels for the discovered categories. In more detail, the GCD baseline uses only one of the two losses used by SimGCD, performing contrastive learning on features, followed by simple clustering in the models’ embedding space. To compare SimGCD and GCD, we start from a ResNet18 feature extractor, training it from scratch to avoid the potential biases identified above. We also train a model with full supervision and obtain 99% average performance on Clevr-4 (on independent test data), showing that the backbone has sufficient capacity. In appendix A, we characterise the limitations of SimGCD in detail and propose an extension,  $\mu$ GCD, which we find substantially outperforms SoTA on Clevr-4, as well as on established GCD benchmarks (the SSB [17]). We show Clevr-4 results in table 4, reporting results for ‘All’, ‘Old’ and ‘New’ class subsets.

**Remarks on Clevr-4.** We note that Clevr-4 can find broader applicability in related fields. As examples, the dataset can be used for disentanglement research and as a simple probing set for biases in representation learning. For instance, we find that most of the ImageNet trained models are biased towards *shape* rather than *texture*, which is in contrast to popular findings from Geirhos *et al.* [13]. Furthermore, larger models are often explicitly proposed as ‘all-purpose’ features for ‘any task’ [29]; here we find simple tasks (*e.g.*, *color* or *count* recognition) where initialization with such models hurts performance compared to training from scratch. Note that practical problems (*e.g.*, vehicle re-identification [33] or crowd counting [34]) may require understanding of such aspects of the image.

## 4 Conclusion

In this paper we have proposed a new dataset, Clevr-4, and used it to investigate the problem of Generalized Category Discovery (GCD). This included probing the limitations of unsupervised representations for the task, as well as for identifying weaknesses in existing GCD methods. We further leveraged our findings to propose a simple but performant algorithm,  $\mu$ GCD, which not only only provides gains on Clevr-4, but also sets a new state-of-the-art on established GCD benchmarks.

161 **References**

- 162 [1] Alex Krizhevsky, Ilya Sutskever, and Geoffrey E Hinton. Imagenet classification with deep convolutional  
163 neural networks. In *NeurIPS*, 2012.
- 164 [2] Kaiming He, Xiangyu Zhang, Shaoqing Ren, and Jian Sun. Deep residual learning for image recognition.  
165 In *CVPR*, 2016.
- 166 [3] Zhuang Liu, Hanzi Mao, Chao-Yuan Wu, Christoph Feichtenhofer, Trevor Darrell, and Saining Xie. A  
167 convnet for the 2020s. In *CVPR*, 2022.
- 168 [4] Susan Carey. *The Origin of Concepts*. Oxford University Press, 2009.
- 169 [5] Gregory Murphy. *The Big Book of Concepts*. Boston Review, 2002.
- 170 [6] Dedre Gentner and Linsey Smith. Analogical reasoning. *Encyclopedia of human behavior*, 2012.
- 171 [7] Sagar Vaze, Kai Han, Andrea Vedaldi, and Andrew Zisserman. Generalized category discovery. In *IEEE  
172 Conference on Computer Vision and Pattern Recognition*, 2022.
- 173 [8] Kaidi Cao, Maria Brbic, and Jure Leskovec. Open-world semi-supervised learning. In *International  
174 Conference on Learning Representations*, 2022.
- 175 [9] Mathilde Caron, Ishan Misra, Julien Mairal, Priya Goyal, Piotr Bojanowski, and Armand Joulin. Unsuper-  
176 vised learning of visual features by contrasting cluster assignments. In *NeurIPS*, 2020.
- 177 [10] Xu Ji, João F Henriques, and Andrea Vedaldi. Invariant information clustering for unsupervised image  
178 classification and segmentation. In *ICCV*, 2019.
- 179 [11] Iro Laina, Yuki M Asano, and Andrea Vedaldi. Measuring the interpretability of unsupervised representa-  
180 tions via quantized reversed probing. In *ICLR*, 2022.
- 181 [12] Justin Johnson, Bharath Hariharan, Laurens van der Maaten, Li Fei-Fei, C Lawrence Zitnick, and Ross  
182 Girshick. Clevr: A diagnostic dataset for compositional language and elementary visual reasoning. In  
183 *CVPR*, 2017.
- 184 [13] Robert Geirhos, Patricia Rubisch, Claudio Michaelis, Matthias Bethge, Felix A Wichmann, and Wieland  
185 Brendel. Imagenet-trained cnns are biased towards texture; increasing shape bias improves accuracy and  
186 robustness. *ICLR*, 2019.
- 187 [14] Mathilde Caron, Hugo Touvron, Ishan Misra, Hervé Jégou, Julien Mairal, Piotr Bojanowski, and Armand  
188 Joulin. Emerging properties in self-supervised vision transformers. In *ICCV*, 2021.
- 189 [15] Alec Radford, Jong Wook Kim, Chris Hallacy, Aditya Ramesh, Gabriel Goh, Sandhini Agarwal, Girish  
190 Sastry, Amanda Askell, Pamela Mishkin, Jack Clark, et al. Learning transferable visual models from  
191 natural language supervision. In *ICML*, 2021.
- 192 [16] Aishwarya Kamath, Mannat Singh, Yann LeCun, Ishan Misra, Gabriel Synnaeve, and Nicolas Carion.  
193 Mdetr-modulated detection for end-to-end multi-modal understanding. *ICCV*, 2021.
- 194 [17] Sagar Vaze, Kai Han, Andrea Vedaldi, and Andrew Zisserman. Open-set recognition: A good closed-set  
195 classifier is all you need. In *International Conference on Learning Representations*, 2022.
- 196 [18] Mahmoud Assran, Mathilde Caron, Ishan Misra, Piotr Bojanowski, Armand Joulin, Nicolas Ballas, and  
197 Michael Rabbat. Semi-supervised learning of visual features by non-parametrically predicting view  
198 assignments with support samples. In *ICCV*, 2021.
- 199 [19] Alex Krizhevsky and Geoffrey Hinton. Learning multiple layers of features from tiny images. *Technical  
200 report*, 2009.
- 201 [20] Kai Han, Andrea Vedaldi, and Andrew Zisserman. Learning to discover novel visual categories via deep  
202 transfer clustering. In *ICCV*, 2019.
- 203 [21] Blender Online Community. *Blender - a 3D modelling and rendering package*. Blender Foundation,  
204 Stichting Blender Foundation, Amsterdam, 2018.
- 205 [22] Subhransu Maji, Esa Rahtu, Juho Kannala, Matthew Blaschko, and Andrea Vedaldi. Fine-grained visual  
206 classification of aircraft. *arXiv preprint arXiv:1306.5151*, 2013.
- 207 [23] James MacQueen. Some methods for classification and analysis of multivariate observations. In *Proceed-  
208 ings of the Fifth Berkeley Symposium on Mathematical Statistics and Probability*, 1967.

- 209 [24] Ting Chen, Simon Kornblith, Mohammad Norouzi, and Geoffrey Hinton. A simple framework for  
 210 contrastive learning of visual representations. In *ICML*, 2020.
- 211 [25] Hugo Touvron, Matthieu Cord, Matthijs Douze, Francisco Massa, Alexandre Sablayrolles, and Herve  
 212 Jegou. Training data-efficient image transformers and distillation through attention. In *ICML*, 2021.
- 213 [26] Kaiming He, Xinlei Chen, Saining Xie, Yanghao Li, Piotr Dollár, and Ross Girshick. Masked autoencoders  
 214 are scalable vision learners. In *CVPR*, 2022.
- 215 [27] Xinlei Chen, Haoqi Fan, Ross Girshick, and Kaiming He. Improved baselines with momentum contrastive  
 216 learning. *arXiv preprint arXiv:2003.04297*, 2020.
- 217 [28] Jinghao Zhou, Chen Wei, Huiyu Wang, Wei Shen, Cihang Xie, Alan Yuille, and Tao Kong. ibot: Image  
 218 bert pre-training with online tokenizer. *ICLR*, 2022.
- 219 [29] Maxime Oquab, Timothée Darcet, Theo Moutakanni, Huy V. Vo, Marc Szafraniec, Vasil Khalidov, Pierre  
 220 Fernandez, Daniel Haziza, Francisco Massa, Alaaeldin El-Nouby, Russell Howes, Po-Yao Huang, Hu Xu,  
 221 Vasu Sharma, Shang-Wen Li, Wojciech Galuba, Mike Rabbat, Mido Assran, Nicolas Ballas, Gabriel  
 222 Synnaeve, Ishan Misra, Herve Jegou, Julien Mairal, Patrick Labatut, Armand Joulin, and Piotr Bojanowski.  
 223 Dinov2: Learning robust visual features without supervision, 2023.
- 224 [30] Xin Wen, Bingchen Zhao, and Xiaojuan Qi. A simple parametric classification baseline for generalized  
 225 category discovery. *ArXiv e-prints*, 2022.
- 226 [31] Aaron van den Oord, Yazhe Li, and Oriol Vinyals. Representation learning with contrastive predictive  
 227 coding. *ArXiv e-prints*, 2018.
- 228 [32] Prannay Khosla, Piotr Teterwak, Chen Wang, Aaron Sarna, Yonglong Tian, Phillip Isola, Aaron Maschinot,  
 229 Ce Liu, and Dilip Krishnan. Supervised contrastive learning. *arXiv preprint arXiv:2004.11362*, 2020.
- 230 [33] Hongye Liu, Yonghong Tian, Yaowei Wang, Lu Pang, and Tiejun Huang. Deep relative distance learning:  
 231 Tell the difference between similar vehicles. In *CVPR*, 2016.
- 232 [34] Yingying Zhang, Desen Zhou, Siqin Chen, Shenghua Gao, and Yi Ma. Single-image crowd counting via  
 233 multi-column convolutional neural network. In *CVPR*, 2016.
- 234 [35] Kiat Chuan Tan, Yulong Liu, Barbara Ambrose, Melissa Tulig, and Serge Belongie. The herbarium  
 235 challenge 2019 dataset. In *Workshop on Fine-Grained Visual Categorization*, 2019.
- 236 [36] Antti Tarvainen and Harri Valpola. Mean teachers are better role models: Weight-averaged consistency  
 237 targets improve semi-supervised deep learning results. In *NeurIPS*, 2017.
- 238 [37] Kaiming He, Haoqi Fan, Yuxin Wu, Saining Xie, and Ross Girshick. Momentum contrast for unsupervised  
 239 visual representation learning. In *CVPR*, 2020.
- 240 [38] Jean-Bastien Grill, Florian Strub, Florent Altché, Corentin Tallec, Pierre Richemond, Elena Buchatskaya,  
 241 Carl Doersch, Bernardo Avila Pires, Zhaohan Guo, Mohammad Gheshlaghi Azar, et al. Bootstrap your  
 242 own latent-a new approach to self-supervised learning. *NeurIPS*, 2020.
- 243 [39] Kihyuk Sohn, David Berthelot, Chun-Liang Li, Zizhao Zhang, Nicholas Carlini, Ekin D. Cubuk, Alex  
 244 Kurakin, Han Zhang, and Colin Raffel. Fixmatch: Simplifying semi-supervised learning with consistency  
 245 and confidence. In *NeurIPS*, 2020.
- 246 [40] Spyros Gidaris and Nikos Komodakis. Dynamic few-shot visual learning without forgetting. In *CVPR*,  
 247 2018.
- 248 [41] Mahmoud Assran, Mathilde Caron, Ishan Misra, Piotr Bojanowski, Florian Bordes, Pascal Vincent, Armand  
 249 Joulin, Mike Rabbat, and Nicolas Ballas. Masked siamese networks for label-efficient learning. In *ECCV*,  
 250 2022.
- 251 [42] Enrico Fini, Enver Sangineto, Stéphane Lathuilière, Zhun Zhong, Moin Nabi, and Elisa Ricci. A unified  
 252 objective for novel class discovery. In *ICCV*, 2021.
- 253 [43] Florent Chiaroni, Jose Dolz, Ziko Imtiaz Masud, Amar Mitiche, and Ismail Ben Ayed. Mutual information-  
 254 based generalized category discovery. *ArXiv e-prints*, 2022.
- 255 [44] Kai Han, Sylvestre-Alvise Rebuffi, Sébastien Ehrhardt, Andrea Vedaldi, and Andrew Zisserman. Autonovel:  
 256 Automatically discovering and learning novel visual categories. *IEEE TPAMI*, 2021.
- 257 [45] Yixin Fei, Zhongkai Zhao, Siwei Yang, and Bingchen Zhao. Xcon: Learning with experts for fine-grained  
 258 category discovery. In *BMVC*, 2022.

- 259 [46] Yiyou Sun and Yixuan Li. Opencon: Open-world contrastive learning. In *Transactions on Machine*  
 260 *Learning Research*, 2022.
- 261 [47] Sheng Zhang, Salman Khan, Zhiqiang Shen, Muzammal Naseer, Guangyi Chen, and Fahad Khan. Prompt-  
 262 cal: Contrastive affinity learning via auxiliary prompts for generalized novel category discovery. *ArXiv*  
 263 *e-prints*, 2022.
- 264 [48] Catherine Wah, Steve Branson, Peter Welinder, Pietro Perona, and Serge Belongie. The Caltech-UCSD  
 265 Birds-200-2011 Dataset. Technical Report CNS-TR-2011-001, California Institute of Technology, 2011.
- 266 [49] Jonathan Krause, Michael Stark, Jia Deng, and Li Fei-Fei. 3d object representations for fine-grained  
 267 categorization. In *4th International IEEE Workshop on 3D Representation and Recognition (3dRR-13)*,  
 268 2013.
- 269 [50] Samuel Ritter, David GT Barrett, Adam Santoro, and Matt M Botvinick. Cognitive psychology for deep  
 270 neural networks: A shape bias case study. In *ICML*, 2017.
- 271 [51] David Arthur and Sergei Vassilvitskii. k-means++: the advantages of careful seeding. In *ACM-SIAM*  
 272 *symposium on Discrete algorithms*, 2007.
- 273 [52] Adam Paszke, Sam Gross, Francisco Massa, Adam Lerer, James Bradbury, Gregory Chanan, Trevor Killeen,  
 274 Zeming Lin, Natalia Gimelshein, Luca Antiga, et al. Pytorch: An imperative style, high-performance deep  
 275 learning library. *NeurIPS*, 2019.
- 276 [53] Ilya Loshchilov and Frank Hutter. SGDR: stochastic gradient descent with warm restarts. In *ICLR*, 2017.
- 277 [54] Hervé Abdi and Lynne J Williams. Principal component analysis.
- 278 [55] Neehar Kondapaneni and Pietro Perona. A number sense as an emergent property of the manipulating  
 279 brain. *ArXiv e-prints*, 2020.
- 280 [56] Laurens Van der Maaten and Geoffrey Hinton. Visualizing data using t-sne. *JMLR*, 2008.
- 281 [57] Kai Han, Sylvestre-Alvise Rebuffi, Sébastien Ehrhardt, Andrea Vedaldi, and Andrew Zisserman. Automatically  
 282 discovering and learning new visual categories with ranking statistics. In *ICLR*, 2020.
- 283 [58] Hugo Touvron, Matthieu Cord, Alaaeldin El-Nouby, Jakob Verbeek, and Hervé Jegou. Three things  
 284 everyone should know about vision transformers. *ArXiv e-prints*, 2022.
- 285 [59] Hugo Touvron, Matthieu Cord, and Hervé Jegou. Deit iii: Revenge of the vit. *ECCV*, 2022.
- 286 [60] Terrance DeVries and Graham W Taylor. Improved regularization of convolutional neural networks with  
 287 cutout. *ArXiv e-prints*, 2017.
- 288 [61] Mathilde Caron, Piotr Bojanowski, Armand Joulin, and Matthijs Douze. Deep clustering for unsupervised  
 289 learning of visual features. In *ECCV*, 2018.
- 290 [62] Xinlei Chen, Haoqi Fan, Ross Girshick, and Kaiming He. Improved baselines with momentum contrastive  
 291 learning. *arXiv preprint arXiv:2003.04297*, 2020.
- 292 [63] Ishan Misra, Abhinav Shrivastava, Abhinav Gupta, and Martial Hebert. Cross-stitch networks for multi-task  
 293 learning. In *CVPR*, 2016.
- 294 [64] Carl Doersch, Abhinav Gupta, and Alexei A Efros. Unsupervised visual representation learning by context  
 295 prediction. In *ICCV*, 2015.
- 296 [65] Ranjay Krishna, Yuke Zhu, Oliver Groth, Justin Johnson, Kenji Hata, Joshua Kravitz, Stephanie Chen,  
 297 Yannis Kalantidis, Li-Jia Li, David A Shamma, et al. Visual genome: Connecting language and vision  
 298 using crowdsourced dense image annotations. *IJCV*, 2017.
- 299 [66] Khoi Pham, Kushal Kafle, Zhe Lin, Zihong Ding, Scott Cohen, Quan Tran, and Abhinav Shrivastava.  
 300 Learning to predict visual attributes in the wild. In *CVPR*, June 2021.
- 301 [67] Irina Higgins, Loic Matthey, Arka Pal, Christopher Burgess, Xavier Glorot, Matthew Botvinick, Shakir  
 302 Mohamed, and Alexander Lerchner. beta-vae: Learning basic visual concepts with a constrained variational  
 303 framework. In *ICLR*, 2017.
- 304 [68] Francesco Locatello, Michael Tschanen, Stefan Bauer, Gunnar Rätsch, Bernhard Schölkopf, and Olivier  
 305 Bachem. Disentangling factors of variation using few labels. *ICLR*, 2020.
- 306 [69] Brooks Paige, Jan-Willem van de Meent, Alban Desmaison, Noah Goodman, Pushmeet Kohli, Frank  
 307 Wood, Philip Torr, et al. Learning disentangled representations with semi-supervised deep generative  
 308 models. *NeurIPS*, 2017.

- 309 [70] Scott E Reed, Yi Zhang, Yuting Zhang, and Honglak Lee. Deep visual analogy-making. *NeurIPS*, 2015.
- 310 [71] Hyunjik Kim and Andriy Mnih. Disentangling by factorising. In *ICML*, 2018.
- 311 [72] Catherine Wah, Steve Branson, Peter Welinder, Pietro Perona, and Serge Belongie. The caltech-ucsd  
312 birds-200-2011 dataset. *Technical Report CNS-TR-2011-001, California Institute of Technology*, 2011.
- 313 [73] Ziwei Liu, Ping Luo, Xiaogang Wang, and Xiaoou Tang. Deep learning face attributes in the wild. In  
314 *ICCV*, 2015.
- 315 [74] Olivia Wiles, Sven Gowal, Florian Stimberg, Sylvestre Alvise-Rebuffi, Ira Ktena, Krishnamurthy Dvi-  
316 jotham, and Taylan Cemgil. A fine-grained analysis on distribution shift. *ICLR*, 2022.
- 317 [75] Zhun Zhong, Enrico Fini, Subhankar Roy, Zhiming Luo, Elisa Ricci, and Nicu Sebe. Neighborhood  
318 contrastive learning for novel class discovery. In *ICCV*, 2021.
- 319 [76] Bingchen Zhao and Kai Han. Novel visual category discovery with dual ranking statistics and mutual  
320 knowledge distillation. In *NeurIPS*, 2021.
- 321 [77] Chuang Niu, Hongming Shan, and Ge Wang. Spice: Semantic pseudo-labeling for image clustering. *IEEE  
322 Transactions on Image Processing*, 2022.
- 323 [78] Grant Van Horn, Oisin Mac Aodha, Yang Song, Yin Cui, Chen Sun, Alex Shepard, Hartwig Adam, Pietro  
324 Perona, and Serge Belongie. The inaturalist species classification and detection dataset. In *CVPR*, 2018.
- 325 [79] Wenbin An, Feng Tian, Ping Chen, Siliang Tang, Qinghua Zheng, and QianYing Wang. Fine-grained  
326 category discovery under coarse-grained supervision with hierarchical weighted self-contrastive learning.  
327 *EMNLP*, 2022.
- 328 [80] Laurynas Karazija, Iro Laina, and Christian Rupprecht. Clevrtex: A texture-rich benchmark for unsuper-  
329 vised multi-object segmentation. In *Proceedings of the Neural Information Processing Systems Track on  
330 Datasets and Benchmarks*, 2021.
- 331 [81] Zhuowan Li, Xingrui Wang, Elias Stengel-Eskin, Adam Kortylewski, Wufei Ma, Benjamin Van Durme,  
332 and Alan L Yuille. Super-clevr: A virtual benchmark to diagnose domain robustness in visual reasoning.  
333 In *CVPR*, 2023.
- 334 [82] Leonard Salewski, A Sophia Koepke, Hendrik PA Lensch, and Zeynep Akata. Clevr-x: A visual reasoning  
335 dataset for natural language explanations. In *xxAI - Beyond explainable Artificial Intelligence*, 2020.
- 336 [83] Sagar Vaze, Nicolas Carion, and Ishan Misra. Genecis: A benchmark for general conditional image  
337 similarity. In *CVPR*, 2023.
- 338 [84] Reuben Tan, Mariya I. Vasileva, Kate Saenko, and Bryan A. Plummer. Learning similarity conditions  
339 without explicit supervision. In *ICCV*, 2019.
- 340 [85] Ishan Nigam, Pavel Tokmakov, and Deva Ramanan. Towards latent attribute discovery from triplet  
341 similarities. In *ICCV*, 2019.
- 342 [86] Jiawei Yao, Enbei Liu, Maham Rashid, and Juhua Hu. Augdmc: Data augmentation guided deep multiple  
343 clustering. *ArXiv e-prints*, 2023.
- 344 [87] Liangrui Ren, Guoxian Yu, Jun Wang, Lei Liu, Carlotta Domeniconi, and Xiangliang Zhang. A diversified  
345 attention model for interpretable multiple clusterings. *TKDE*, 2022.
- 346 [88] Ruchika Chavhan, Henry Gouk, Jan Stuehmer, Calum Heggan, Mehrdad Yaghoobi, and Timothy  
347 Hospedales. Amortised invariance learning for contrastive self-supervision. *ICLR*, 2023.
- 348 [89] Linus Ericsson, Henry Gouk, and Timothy M Hospedales. Why do self-supervised models transfer?  
349 investigating the impact of invariance on downstream tasks. *ArXiv e-prints*, 2021.
- 350 [90] Ravid Shwartz-Ziv, Randall Balestrierio, and Yann LeCun. What do we maximize in self-supervised  
351 learning?, 2022.
- 352 [91] Randall Balestrierio, Ishan Misra, and Yann LeCun. A data-augmentation is worth a thousand samples:  
353 Analytical moments and sampling-free training. In *NeurIPS*, 2022.
- 354 [92] Yann Dubois, Stefano Ermon, Tatsunori B Hashimoto, and Percy S Liang. Improving self-supervised  
355 learning by characterizing idealized representations. *NeurIPS*, 2022.
- 356 [93] Wenbin An, Feng Tian, Qinghua Zheng, Wei Ding, QianYing Wang, and Ping Chen. Generalized category  
357 discovery with decoupled prototypical network. *AAAI*, 2023.

358 **Appendices**

359 We summarize the appendices in the Contents table below, particularly highlighting: appendix A for  
360 details on our proposed  $\mu$ GCD method; appendices C.1 and C.2 for details on Clevr-4; appendix E.3  
361 for a long-tail evaluation of  $\mu$ GCD on the Herbarium19 dataset [35]; and appendix D.5 for analysis  
362 on the use of cosine classifiers in GCD.

363	<b>A The <math>\mu</math>GCD algorithm</b>	<b>9</b>
364	A.1 Addressing limitations in current approaches . . . . .	10
365	A.2 Our method . . . . .	10
366	<b>B Results on real data and further analysis</b>	<b>11</b>
367	<b>C Clevr-4</b>	<b>12</b>
368	C.1 Clevr-4 generation . . . . .	12
369	C.2 Clevr-4 details . . . . .	13
370	C.3 Clevr-4 examples . . . . .	13
371	<b>D Analysis of results</b>	<b>14</b>
372	D.1 Clevr-4 error bars . . . . .	14
373	D.2 <i>shape</i> failure case . . . . .	14
374	D.3 Semi-supervised $k$ -means with pre-trained backbones . . . . .	16
375	D.4 Clustering with sub-spaces of pre-trained features . . . . .	16
376	D.5 Understanding cosine classifiers in category discovery . . . . .	17
377	D.6 Design of data augmentation and mis-aligned augmentations . . . . .	19
378	D.7 Effect of $\lambda_1$ . . . . .	20
379	<b>E Additional Experiments</b>	<b>20</b>
380	E.1 Results with estimated number of classes . . . . .	20
381	E.2 Results with varying proportion of labelled examples . . . . .	21
382	E.3 Results on Herbarium19 . . . . .	21
383	<b>F Description of baselines and <math>\mu</math>GCD algorithms</b>	<b>21</b>
384	<b>G Further Implementation Details</b>	<b>23</b>
385	<b>H Related Work</b>	<b>25</b>
386	H.1 Clevr-4: connections to real-world and disentanglement datasets . . . . .	25
387	H.2 $\mu$ GCD method. . . . .	26
388	<b>A The <math>\mu</math>GCD algorithm</b>	

389 Observing results in table 4, we make the three following observations regarding the performance of  
390 existing methods on Clevr-4: **(i)** Both methods’ performance on *texture* and *count* is substantially  
391 worse than on *shape* and *color*. **(ii)** On the harder *texture* and *count* splits, the GCD baseline actually  
392 outperforms the SimGCD state-of-the-art. Given that SimGCD differs from GCD by adding a  
393 classification head and corresponding loss, this indicates that jointly training classifier and feature-  
394 space losses can hurt performance. **(iii)** Upon closer inspection, we find that the main performance

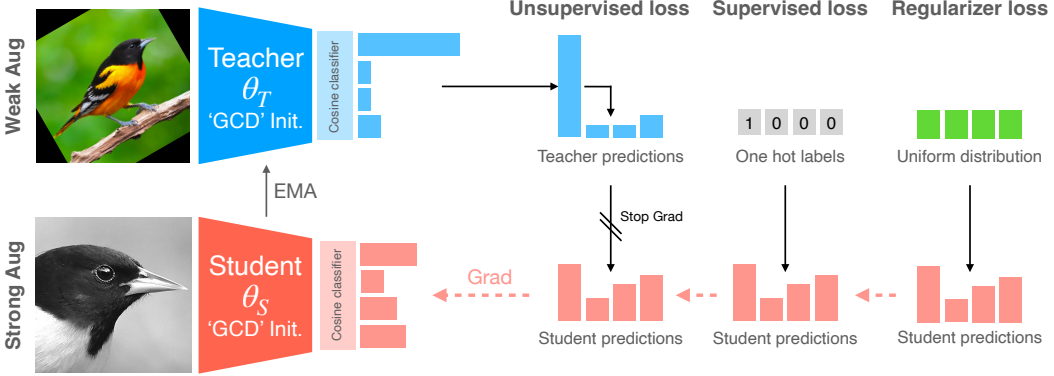


Figure 2: **Our ‘ $\mu$ GCD’ method.** We begin with representation learning from the GCD baseline, followed by finetuning in a mean-teacher style setup. Here, a ‘teacher’ provides supervision for a ‘student’ network, and maintains parameters as the exponential moving average (EMA) of the student.

395 gap on *texture* and *count* comes from accuracy on the ‘New’ categories; both methods cluster the  
 396 ‘Old’ categories almost perfectly. This suggests that the ‘New’ class pseudo-labels from SimGCD are  
 397 not strong enough; GCD, with no (pseudo-)supervision for novel classes, achieves higher clustering  
 398 performance.

### 399 A.1 Addressing limitations in current approaches

400 Given these findings, we seek to improve the quality of the pseudo-labels for ‘New’ categories.  
 401 Specifically, we draw inspiration from the mean-teacher setup for semi-supervised learning [36],  
 402 which has been adapted with minor changes in many self-supervised frameworks [14, 37, 38]. Here,  
 403 a ‘student’ network is supervised by class pseudo-labels generated by a ‘teacher’. The teacher is an  
 404 identical architecture with parameters updated with the Exponential Moving Average (EMA) of the  
 405 student. The intuition is that the slowly updated teacher is more robust to the noisy supervision from  
 406 pseudo-labels, which in turn improves the quality of the pseudo-labels themselves. Also, rather than  
 407 *jointly optimizing* both SimGCD losses, we first train the backbone *only* with the GCD baseline loss,  
 408 before *finetuning* with the classification head and loss.

409 These changes, together with careful consideration of the data augmentations, give rise to our  
 410 proposed  $\mu$ GCD (mean-GCD) algorithm, which we fully describe next in appendix A. Here, we note  
 411 the improvements that this algorithm brings in Clevr-4 on the bottom line of table 4. Overall,  $\mu$ GCD  
 412 outperforms SimGCD on three of the four Clevr-4 taxonomies, and further outperforms SimGCD by  
 413 nearly 5% on average across all splits.  $\mu$ GCD underperforms SimGCD on the *shape* split of Clevr-4  
 414 and we analyse this failure case in the supplementary.

### 415 A.2 Our method

416 In this section, we detail a simple but strong method for GCD,  $\mu$ GCD, already motivated in section 3  
 417 and illustrated in fig. 2. In a first phase, the algorithm proceeds in the same way as the GCD  
 418 baseline [7], learning the representation. Next, we append a classification head and fine-tune the  
 419 model with a ‘mean teacher’ setup [36], similarly to SimGCD but yielding more robust pseudo-labels.

420 Concretely, we construct models,  $f_\theta$ , as the composition of a feature extractor,  $\Phi$ , and a classification  
 421 head,  $g$ .  $\Phi$  is first trained with the representation learning framework from [7] as described above,  
 422 and the composed model gives  $f = g \circ \Phi$  with values in  $\mathbb{R}^k$ , where  $k$  is the total number of categories  
 423 in the dataset. Next, we sample a batch of images,  $\mathcal{B}$ , and generate two random augmentations of  
 424 every instance. We pass one view through the student network  $f_{\theta_S}$ , and the other through the teacher  
 425 network  $f_{\theta_T}$ , where  $\theta_S$  and  $\theta_T$  are the network parameters of the student and teacher, respectively.  
 426 We compute the cross-entropy loss between the (soft) teacher pseudo-labels and student predictions:

$$\mathcal{L}^u(\theta_S; \mathcal{B}) = -\frac{1}{|\mathcal{B}|} \sum_{x \in \mathcal{B}} \langle \mathbf{p}_T(x), \log(\mathbf{p}_S(x)) \rangle, \quad \mathbf{p}_*(x) = \text{softmax}(f_{\theta_*}(x); \tau_*), \quad (1)$$

427 where  $\mathbf{p}_*(x) \in [0, 1]^k$  are the softmax outputs of the student and teacher networks, scaled with  
 428 temperature  $\tau_*$ . We further use labelled instances in the batch with a supervised cross-entropy

Table 5: **Category discovery accuracy (ACC) on the Semantic Shift Benchmark [17].** We report results from prior work using DINO initialization [14], and reimplement GCD baselines and SimGCD with DINOv2 pre-training [29] (noted with \*). MIB [43] and SimGCD [30] are recent pre-prints.

Pre-training		CUB			Stanford Cars			Aircraft			Average
		All	Old	New	All	Old	New	All	Old	New	
<i>k</i> -means [23]	DINO	34.3	38.9	32.1	12.8	10.6	13.8	16.0	14.4	16.8	21.1
RankStats+ [44]	DINO	33.3	51.6	24.2	28.3	61.8	12.1	26.9	36.4	22.2	29.5
UNO+ [42]	DINO	35.1	49.0	28.1	35.5	70.5	18.6	40.3	56.4	32.2	37.0
ORCA [8]	DINO	35.3	45.6	30.2	23.5	50.1	10.7	22.0	31.8	17.1	26.9
GCD [7]	DINO	51.3	56.6	48.7	39.0	57.6	29.9	45.0	41.1	46.9	45.1
XCon [45]	DINO	52.1	54.3	51.0	40.5	58.8	31.7	47.7	44.4	49.4	46.8
OpenCon [46]	DINO	54.7	63.8	54.7	49.1	78.6	32.7	-	-	-	-
MIB [43]	DINO	62.7	75.7	56.2	43.1	66.9	31.6	-	-	-	-
PromptCAL [47]	DINO	62.9	64.4	62.1	50.2	70.1	40.6	52.2	52.2	52.3	55.1
SimGCD [30]	DINO	60.3	65.6	57.7	53.8	71.9	45.0	54.2	59.1	51.8	56.1
$\mu$ GCD (Ours)	DINO	65.7	68.0	64.6	56.5	68.1	50.9	53.8	55.4	53.0	58.7
<i>k</i> -means*	DINOv2	67.6	60.6	71.1	29.4	24.5	31.8	18.9	16.9	19.9	38.6
GCD*	DINOv2	71.9	71.2	72.3	65.7	67.8	64.7	55.4	47.9	59.2	64.3
SimGCD*	DINOv2	71.5	<b>78.1</b>	68.3	71.5	81.9	66.6	63.9	<b>69.9</b>	60.9	69.0
$\mu$ GCD (Ours)	DINOv2	<b>74.0</b>	75.9	<b>73.1</b>	<b>76.1</b>	<b>91.0</b>	<b>68.9</b>	<b>66.3</b>	68.7	<b>65.1</b>	<b>72.1</b>

429 component as:

$$\mathcal{L}^s(\theta_S; \mathcal{B}_L) = -\frac{1}{|\mathcal{B}_L|} \sum_{i \in \mathcal{B}_L} \langle \mathbf{y}(\mathbf{x}), \log(\mathbf{p}_S(\mathbf{x})) \rangle, \quad (2)$$

430 where  $\mathcal{B}_L \in \mathcal{B}$  is the labelled subset of the batch and  $\mathbf{y}(\mathbf{x}) \in \{0, 1\}^k$  is the one-hot class label of  
431 the example  $\mathbf{x}$ . Finally, we add a mean-entropy maximization regularizer from [18] to encourage  
432 pseudo-labels for all categories:

$$\mathcal{L}^r(\theta_S) = -\langle \bar{\mathbf{p}}_S, \log(\bar{\mathbf{p}}_S) \rangle, \quad \bar{\mathbf{p}}_S = \frac{1}{|\mathcal{B}|} \sum_{\mathbf{x} \in \mathcal{B}} \mathbf{p}_S(\mathbf{x}). \quad (3)$$

433 The student is trained with respect to the following total loss, given hyper-parameters  $\lambda_1$  and  $\lambda_2$ :  
434  $\mathcal{L}(\theta_S; \mathcal{B}) = (1 - \lambda_1)\mathcal{L}^u(\theta_S; \mathcal{B}) + \lambda_1\mathcal{L}^s(\theta_S; \mathcal{B}_L) + \lambda_2\mathcal{L}^r(\theta_S)$ . The teacher parameters are updated  
435 as the moving average  $\theta_T = \omega(t)\theta_T + (1 - \omega(t))\theta_S$ , where  $\omega(t)$  is a time-varying momentum.

436 **Augmentations.** While often regarded as an ‘implementation detail’, an important component of our  
437 method is the careful consideration of augmentations used in the computation of  $\mathcal{L}^u$ . Specifically,  
438 on the SSB, we pass different views of the same instance to the student and teacher networks. We  
439 generate a *strong* augmentation which is passed to the student network, and a *weak* augmentation  
440 which is passed to the teacher, similarly to [39]. The intuition is that, while contrastive learning  
441 benefits from strong data augmentations [9, 14], we wish the teacher network’s predictions to be  
442 as stable as possible. Meanwhile, on Clevr-4, misaligned data augmentations — *e.g.*, aggressive  
443 cropping for *count*, or color jitter for *color* — substantially degrade performance (see appendix D.6).

444 **Architecture.** We adopt a ‘cosine classifier’ as  $g$ , which was introduced in [40] and leverages  $L^2$ -  
445 normalized weight vectors and feature representations. While it has been broadly adopted for many  
446 tasks [8, 9, 30, 41, 42], we demonstrate *why* this component helps in the supplementary. We find that  
447 normalized vectors are important to avoid collapse of the predictions to the labelled categories.

## 448 B Results on real data and further analysis

449 **Datasets.** We compare  $\mu$ GCD against prior work on the standard Semantic Shift Benchmark (SSB)  
450 suite [17]. The SSB comprises three fine-grained evaluations: CUB [48], Stanford Cars [49] and  
451 FGVC-Aircraft [22]. Though the SSB datasets do not contain independent clusterings of the same  
452 images (as in Clevr-4) the evaluations do have well-defined taxonomies — *i.e.* birds, cars and aircrafts.  
453 Furthermore, the SSB contains curated novel class splits which control for semantic distance with the  
454 labelled set. We find that coarse-grained GCD benchmarks do not specify clear taxonomies in the  
455 labelled set, and we include a long-tailed evaluation on Herbarium19 [35] in the supplementary.

456 **Model initialization and compared methods.** The SSB contains fine-grained, object-centric datasets,  
457 which have been shown to benefit from greater shape bias [50]. Prior GCD methods [7, 45, 46]

458 initialize with DINO [14] pre-training, which we show in table 2 had the strongest shape bias among  
 459 self-supervised models. However, the recent DINOv2 [29] demonstrates a substantially greater shape  
 460 bias. As such, we train our model both with DINO and DINOv2 initialization, further re-implementing  
 461 GCD baselines [7, 51] and SimGCD [30] with DINOv2 for comparison.

462 **Implementation details.** We implement all models in PyTorch [52] on a single NVIDIA P40 or M40.  
 463 Most models are trained with an initial learning rate of 0.1 which is decayed with a cosine annealed  
 464 schedule [53]. For our EMA schedule, we ramp it up throughout training with a cosine function [38]:  
 465  $\omega(t) = \omega_T - (1 - \omega_{base})(\cos(\frac{\pi t}{T}) + 1)/2$ . Here  $t$  is the current epoch and  $T$  is the total number of  
 466 epochs. Differently, however, to most self-supervised learning literature [38], we found a much lower  
 467 initial decay to be beneficial; we ramp up the decay from  $\omega_{base} = 0.7$  to  $\omega_T = 0.999$  during training.  
 468 Further implementation details can be found in the supplementary.

469 **Discussion of results (table 5).** Overall, we find that  $\mu$ GCD outperforms the existing state-of-the-art,  
 470 SimGCD [30], by over 2% on average across all SSB evaluations when using DINO initialization.  
 471 When using the stronger DINOv2 backbone, we find that the performance of the simple  $k$ -means  
 472 baseline nearly doubles in accuracy, substantiating our choice of shape-biased initialization on this  
 473 object-centric evaluation. The gap between the GCD baseline [7] and the SimGCD state-of-the-  
 474 art [30] is also reduced from over 10% to under 5% on average. Nonetheless, our method outperforms  
 475 SimGCD by over 3% on average, as well as on each dataset individually, setting a new state-of-the-art.

476 **Ablations.** We ablate our main design choices in table 6. L(1) shows the importance of pre-  
 477 training with the GCD baseline loss [7] (though we find in section 3 that jointly training this  
 478 loss with the classifier, as in SimGCD [30], is difficult). L(2) further demonstrates that stronger  
 479 augmentation for the student network is critical, with a 7% drop in CUB performance without  
 480 it. L(3)-(5) highlight the importance of a carefully designed EMA schedule, our use of a time-  
 481 varying decay outperforms constant decay values. This is intuitive as early on in training, with a  
 482 randomly initialized classification head, we wish for the teacher to be updated quickly. Later on  
 483 in training, slow teacher updates mitigate the effect of noisy pseudo-labels within any given batch.  
 484 Furthermore, in L(6)-(7), we validate the importance of entropy regularization and cosine classifiers  
 485 in category discovery. In the supplementary, we provide evidence as to *why* these commonly used  
 486 components [8, 30, 42] are necessary, and also discuss the design of the student augmentation.  
 487

488 **PCA Visualization.** Finally, we perform anal-  
 489 ysis on the *count* split of Clevr-4. Uniquely  
 490 amongst the four taxonomies, the *count* cate-  
 491 gories have a clear order. In fig. 3, we plot  
 492 the first two principal components [54] of the  
 493 normalized features of the GCD baseline [7],  
 494 SimGCD [30] and  $\mu$ GCD. It is clear that all fea-  
 495 ture spaces learn a clear ‘number sense’ [55]  
 496 with image features placed in order of increas-  
 497 ing object count. Strikingly, this sense of nu-  
 498 merosity is present even beyond the supervised  
 499 categories (count greater than 5) as a byproduct  
 500 of a simple recognition task. Furthermore, while the baseline learns elliptical clusters for each  
 501 category, SimGCD and  $\mu$ GCD project all images onto a one-dimensional object in feature space.  
 502 This object can be considered as a ‘semantic axis’: a low-dimensional manifold in feature  
 503 space,  $\mathbb{R} \in \mathbb{R}^d$ , along which the category label changes.

## 504 C Clevr-4

### 505 C.1 Clevr-4 generation

506 We build Clevr-4 using Blender [21], a free 3D rendering software with a Python API. Following the  
 507 CLEVR dataset [12], our images are constituted of multiple rendered objects in a static scene. Each  
 508 object is defined by three ‘semantic’ attributes (*texture*, *shape* and *color*), and is further defined by  
 509 its *size*, *pose* and *position* in the scene. We consider the first three attributes as ‘semantic’ as they  
 510 are categorical variables which can neatly define image ‘classes’. Meanwhile, we designate the *size*,  
 511 *pose* and *position* attributes as ‘nuisance’ factors which are not related to the image category.

512 **CLEVR Limitations.** CLEVR is first limited – for the purposes of category discovery – as it has  
 513 only two textures (‘rubber’ and ‘metal’) and three shapes (‘cube’, ‘sphere’ and ‘cylinder’). For

Table 6: **Ablations.** We find that a proper intialization, momentum decay schedule, and augmentation strategy are critical to strong performance.

	CUB		
	All	Old	New
$\mu$ GCD (Ours)	<b>65.7</b>	68.0	<b>64.6</b>
(1) W/o GCD init.	61.7	66.2	59.6
(2) W/o stronger student augmentation	58.1	<b>72.5</b>	50.9
(3) With $\omega_t := 1$	1.6	1.1	1.8
(4) With $\omega_t := 0.0$	62.7	66.4	60.9
(5) With $\omega_t := 0.7$	64.1	65.1	63.6
(6) W/o cosine classifier	54.9	64.2	50.3
(7) W/o ME-Max regularizer	42.0	41.8	42.1

while the baseline learns elliptical clusters for each

category, SimGCD and  $\mu$ GCD project all images onto a one-dimensional object in feature space.

This object can be considered as a ‘semantic axis’: a low-dimensional manifold in feature

space,  $\mathbb{R} \in \mathbb{R}^d$ , along which the category label changes.

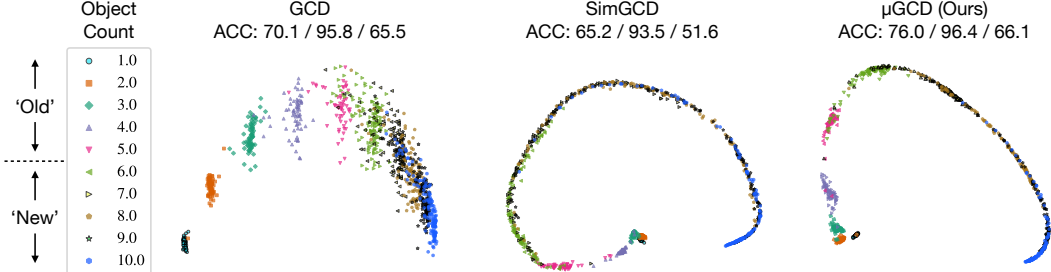


Figure 3: PCA [54] of features from the GCD baseline [7], SimGCD [30] and  $\mu$ GCD on the *count* split of Clevr-4. While the baseline learns elliptical clusters for each category, SimGCD and  $\mu$ GCD project images onto a one-dimensional object in feature space, which be considered as a ‘semantic axis’ along which the category changes. Clustering accuracy is reported for ‘All’/‘Old’/‘New’ classes.

514 category discovery, we wish to have *more* categories, both to increase the difficulty of the task, and to  
 515 ensure a sufficient number of classes in the ‘Old’ and ‘New’ subsets. Furthermore, we wish to have  
 516 the *same* number of categories in each split; otherwise, in principal, an unsupervised algorithm may  
 517 be able to distinguish the taxonomy simply from the number of categories present.

518 **Expanding the taxonomies.** To increase the number of categories in each taxonomy, we introduce  
 519 new textures, colours and shapes to the dataset, resulting in 10 categories for each taxonomy. We  
 520 create most of the *8 new textures* by wrapping a black-and-white JPEG around the surface of the  
 521 object, each of which have their own design (*e.g.*, ‘chessboard’ or ‘circles’). Given an ‘alpha’ for the  
 522 opaqueness of this wrapping, these textures can be distinguished independently of the underlying  
 523 color. We further leverage pre-fabricated meshes packaged with Blender to introduce *7 new shapes* to  
 524 the dataset, along with *2 new colors* for the objects. The new shapes and colors were selected to be  
 525 clearly distinguishable from each other. Full definitions of the taxonomies are given in appendix C.2.

526 **Image sampling process.** For a given image, we first independently sample object *texture*, *shape*  
 527 and *color*. We then randomly sample how many objects should be in the image (*i.e.*, object *count*)  
 528 and place this many objects in the scene. Each object has its own randomly sampled size (which is  
 529 taken to be one of three discrete values), position and relative pose. Thus, differently to CLEVR,  
 530 all objects in the image have the same *texture*, *shape* and *color*. This allows these three attributes,  
 531 together with *count*, to define independent taxonomies within the data.

## 532 C.2 Clevr-4 details

533 We describe the categories in each of the four taxonomies in Clevr-4 below. All taxonomies have  
 534 10 categories, five of which are used in the labeled set and shown in bold. Image exemplars of all  
 535 categories are given in figs. 6 and 7.

- 536     • Texture: **rubber**, **metal**, **checkered**, **emojis**, **wave**, brick, star, circles,  
 537       zigzag, chessboard
- 538     • Shape: **cube**, **sphere**, **monkey**, **cone**, **torus**, star, teapot, diamond, gear,  
 539       cylinder
- 540     • Color: **gray**, **red**, **blue**, **green**, **brown**, purple, cyan, yellow, pink, orange
- 541     • Count: **1**, **2**, **3**, **4**, **5**, 6, 7, 8, 9, 10

542 fig. 5 plots the frequency of all categories in the taxonomies, while fig. 4 shows the mutual information  
 543 between the four taxonomies. We find that all taxonomies, except for *shape*, are roughly balanced,  
 544 and the four taxonomies have approximately no mutual information between them – realizing our  
 545 desire of them being *statistically independent*.

## 546 C.3 Clevr-4 examples

547 We give examples of each of the four taxonomies in Clevr-4 in figs. 6 and 7.

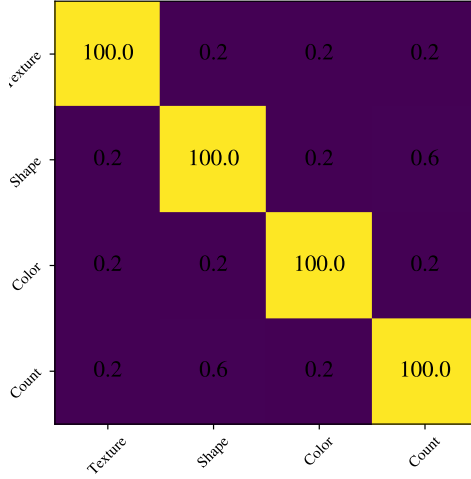


Figure 4: **Normalized mutual information** between the four taxonomies in Clevr-4. All taxonomies have roughly no mutual information between them (they are statistically independent).

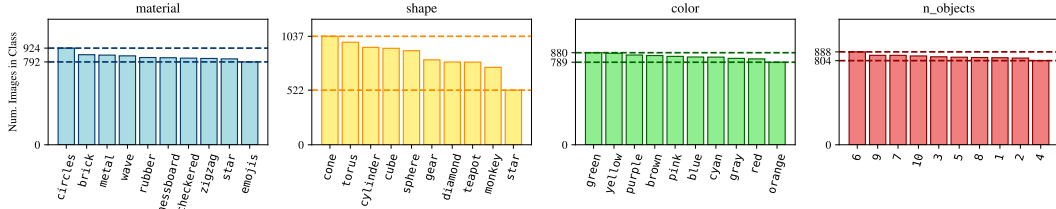


Figure 5: **Category frequency plots** for each taxonomy in Clevr-4. All taxonomies are roughly balanced, except for *shape*. *shape* shows minor imbalance due to greater difficulty in placing many objects of some shapes (e.g., ‘star’ and ‘monkey’).

## 548 D Analysis of results

### 549 D.1 Clevr-4 error bars

550 We show results for the GCD baseline [7], the current state-of-the-art SimGCD [30] and our method,  
551  $\mu$ GCD, in fig. 8. The results are shown for five random seeds for each method, and plotted with the  
552 standard `matplotlib` boxplot function, which identifies outliers in colored circles. We also plot the  
553 *median* performance of our method on each taxonomy in dashed lines.

554 Broadly speaking, the takeaways are the same as the results from Table 4 of the main paper. However,  
555 while the *mean* performance of our method is worse than SimGCD on the *shape* split, we can see here  
556 that the median performance of  $\mu$ GCD is *within bounds, or significantly better*, than the compared  
557 methods on *all taxonomies*.

### 558 D.2 *shape* failure case

559 Overall, we find our proposed  $\mu$ GCD outperforms prior state-of-the-art methods on three of the four  
560 Clevr-4 splits (as well as on the Semantic Shift Benchmark [17]). We further show in appendix D.1  
561 that, when accounting for outliers in the five random seeds, our method is also roughly equivalent to  
562 the SimGCD [30] state-of-the-art on the *shape* split of Clevr-4.

563 Nonetheless, we generally find that our method is less stable on the *shape* split of Clevr-4 than on  
564 other taxonomies and datasets. We provide some intuitions for this by visualizing the representations  
565 and predictions of our method in fig. 9.

566 **Preliminaries:** In fig. 9, we plot TSNE projections [56] of the feature spaces of two versions of  
567 our model, as well as the histograms of the models’ predictions on the *shape* split. Along with the  
568 models’ image representations (colored scatter points), we also plot the class vectors of the cosine  
569 classifiers (colored stars). On the left, we show our trained model when we randomly initialize  
570 the cosine classifier, while on the right we initialize the class vectors in the classifier with *k*-means  
571 centroids. We derive these centroids by running standard *k*-means on the image embeddings of the  
572 backbone, which is pre-trained with the GCD-style representation learning step (see appendix F).

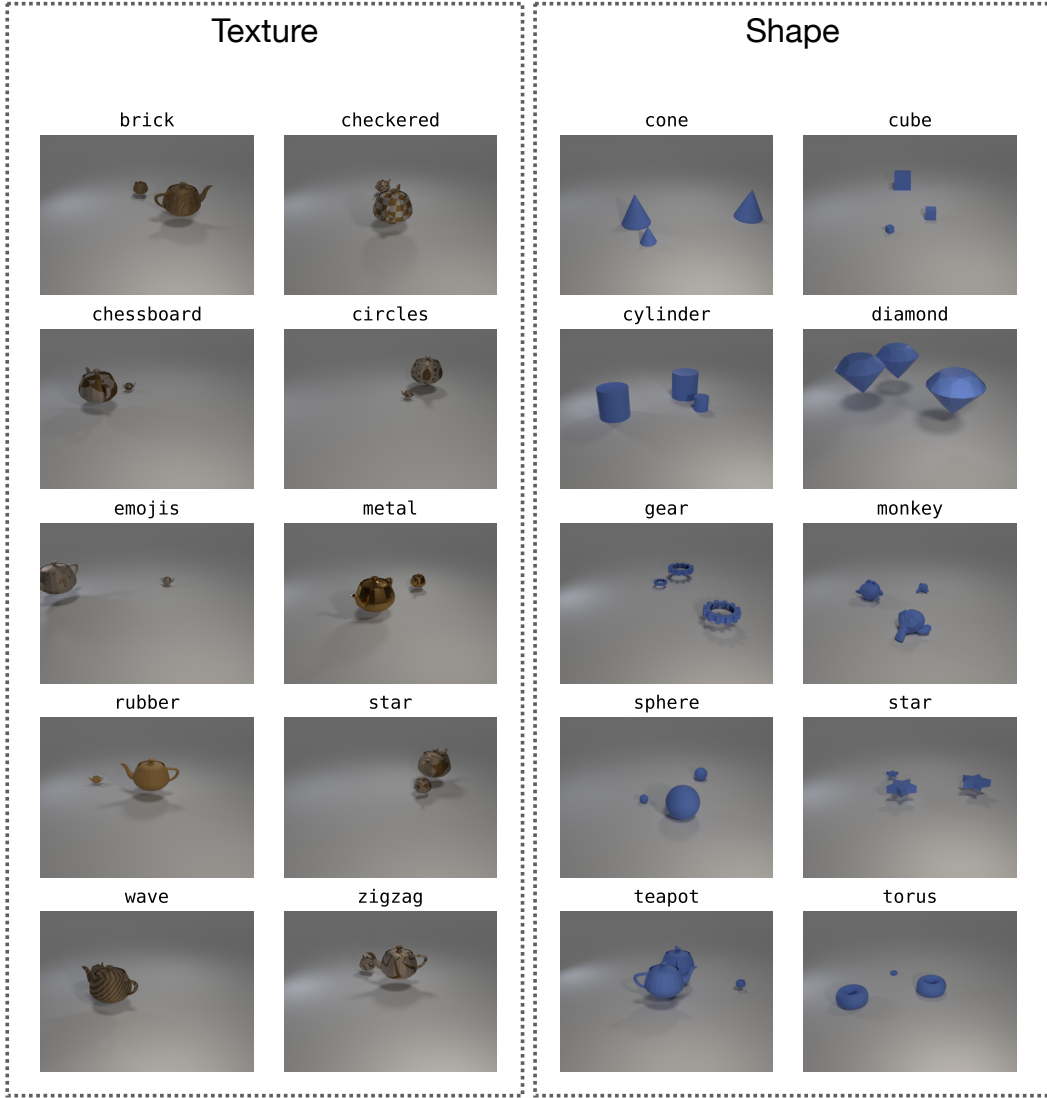


Figure 6: **Examples of each category** from the *texture* and *shape* taxonomies of Clevr-4.

573 **Observations:** In the plot on the **left**, we find that though the feature space is very well separated  
 574 (there is little overlap between clusters of different categories), the performance of the classifier is  
 575 still only around 90%. The histogram of model predictions demonstrates that this is due to no images  
 576 being assigned to the ‘star’ category – this vector in the classifier is completely unused. Instead, too  
 577 many instances are assigned to ‘gear’. In the TSNE plot, we can see that the ‘gear’ class vector is  
 578 between clusters for both ‘gear’ and ‘star’ images, while the ‘star’ vector is pushed far away from  
 579 both. We suggest that this is due to the optimization falling into a local optimum early on in training,  
 580 as a result of the feature-space initialization already being so strong.

581 On the **right**, we find we can largely alleviate this problem by initializing the classification head  
 582 carefully – with  $k$ -means centroids from the pre-trained backbone. We see that the problem is nearly  
 583 perfectly solved, and the histogram of predictions reflects the true class distribution of the labels.

584 **Takeaway:** We find that when the initialization of the model’s backbone – from the GCD-style  
 585 representation learning step, see appendix F – is already very strong, random initialization of the  
 586 classification head in  $\mu$ GCD can result in local optima in the model’s optimization process. This can  
 587 be alleviated by initializing the classification head carefully with  $k$ -means centroids – resulting in  
 588 almost perfect performance – but the issue can persist with some random seeds (see appendix D.1).

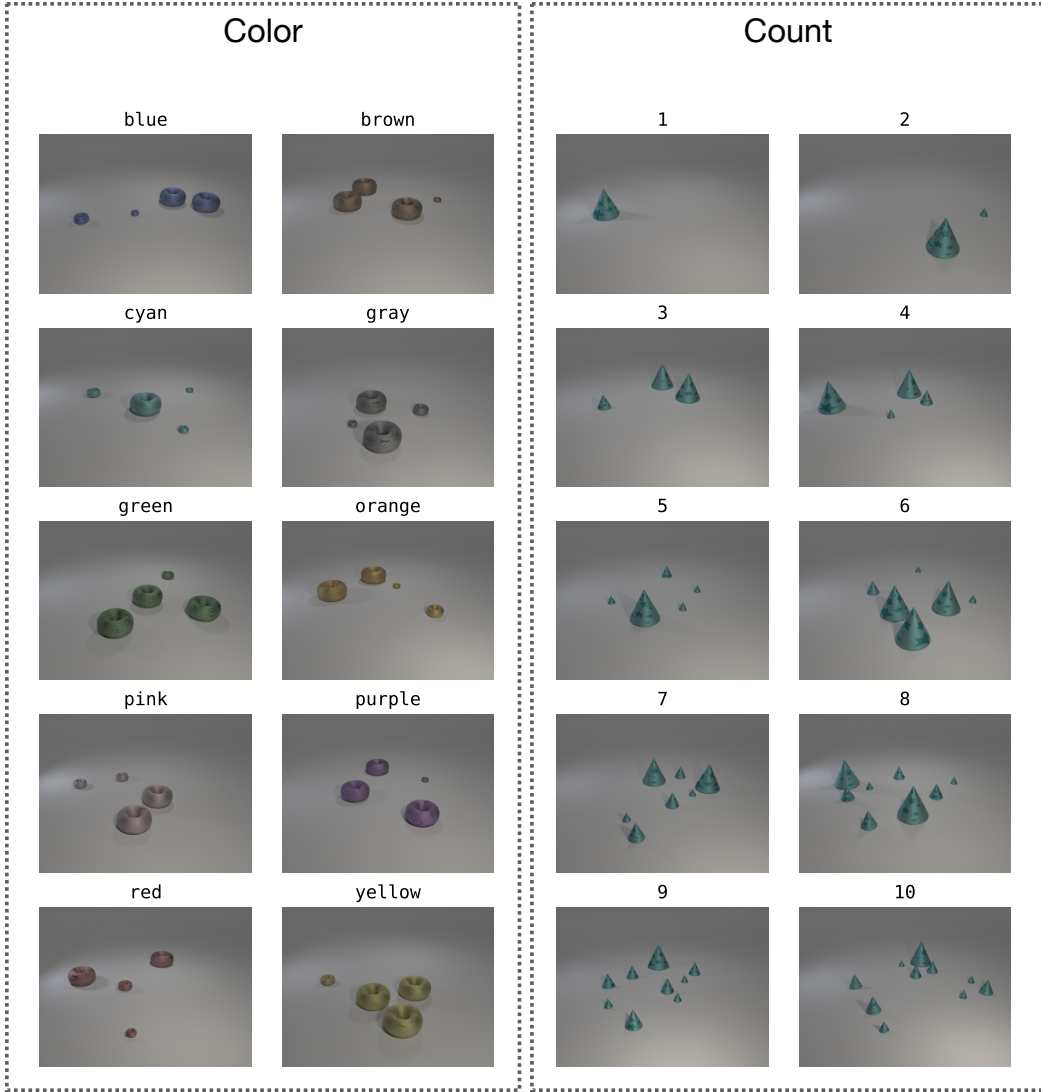


Figure 7: Examples of each category from the *color* and *count* taxonomies of Clevr-4.

### 589 D.3 Semi-supervised $k$ -means with pre-trained backbones

590 In fig. 10, we probe the effect of running semi-supervised  $k$ -means [7] on top of different pre-trained  
 591 backbones. This is a simple mechanism by which models can leverage the information from the  
 592 ‘Old’ class labels. We find that while this improves clustering performance on some taxonomies, it is  
 593 insufficient to overcome the biases learned during the models’ pretraining, corroborating our findings  
 594 from table 2 of the main paper.

### 595 D.4 Clustering with sub-spaces of pre-trained features

596 In table 2 and fig. 10, we demonstrate that all pre-trained models have a clear bias towards one of the  
 597 Clevr-4 taxonomies. Specifically, we find that clustering in pre-trained feature spaces preferentially  
 598 aligns with a single attribute (e.g *shape* or *color*).

599 Here, we investigate whether these clusters have any sub-structures. To do this, we perform PCA  
 600 analysis on features extracted with two backbones: DINoV2 [29] and MAE [26]. Intuitively, we  
 601 wish to probe whether the omission of dominant features from the backbones (e.g the *shape* direction  
 602 with DINoV2 features) allows  $k$ -means clustering to identify other taxonomies. Specifically, we:  
 603 (i) extract features for all images using a given backbone,  $\mathbf{X} \in \mathbb{R}^{N \times D}$ ; (ii) identify the principal  
 604 components of the features, sorted by their component scores,  $\mathbf{W} \in \mathbb{R}^{D \times D}$ ; (iii) re-project the

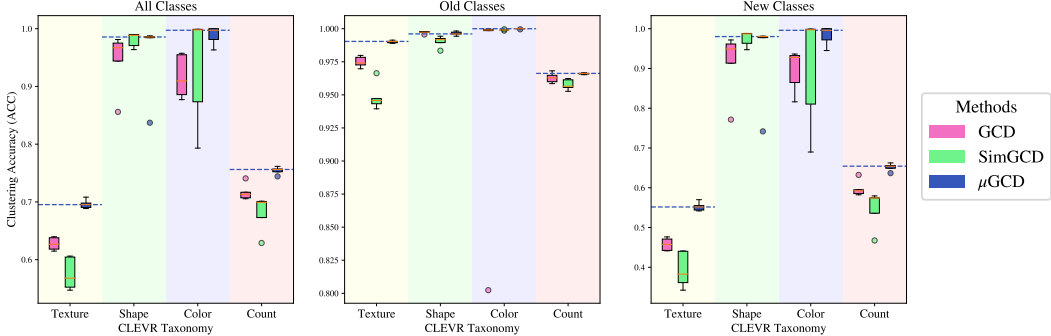


Figure 8: **Box plots of results on Clevr-4.** We show results for the GCD baseline [7], the current state-of-the-art SimGCD [30] and our method,  $\mu$ GCD. We plot results for five random seeds for the four taxonomies, with outliers shown as colored circles. We also plot the median performance of our method on each taxonomy in dashed lines. On all taxonomies,  $\mu$ GCD is within bounds, or significantly better, than the compared methods.

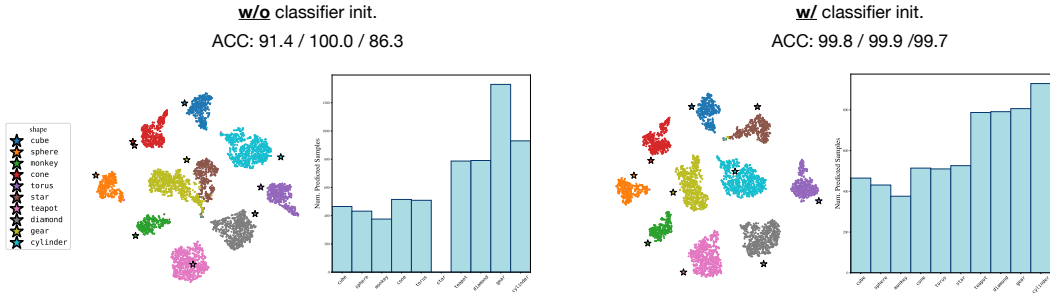


Figure 9: **Analysis of the shape failure mode**, showing TSNE plots [56] and prediction histograms for two models, trained *without* (left) and *with* (right) initialization of the classification head with  $k$ -means centroids. **Left:** When the backbone initialization (from the GCD representation learning step [7]) is already very strong, the classification head gets stuck in a local optimum, with one class vector unused. **Right:** We find we can alleviate this by initializing the class vectors with  $k$ -means centroids, almost perfectly solving the problem, but the issue can persist with some random seeds.

605 features onto the components, omitting those with the  $p$  highest scores,  $\hat{\mathbf{X}} = (\mathbf{X} - \mu) \cdot \mathbf{W}[:, p:]$ ; (iv)  
606 cluster the resulting features,  $\hat{\mathbf{X}} \in \mathbb{R}^{N \times D-p}$ , with  $k$ -means. Here,  $\mu$  is the average of the features  $\mathbf{X}$ ,  
607 and the results are shown in figs. 11 and 12.

608 Overall, we find that by removing the dominant features from the backbones, performance on other  
609 taxonomies can be improved (at the expense of performance on the ‘dominant’ taxonomy). The effect  
610 is particularly striking with MAE, where we see an almost seven-fold increase in *shape* performance  
611 after the three most dominant principal components are removed.

612 This aligns with the reported performance characteristics of DINOv2 and MAE. The object-centric  
613 recognition datasets on which these models are evaluated benefit from *shape*-biased representations  
614 (see appendix B). We find here that both MAE and DINOv2 encode shape information, but that more  
615 work is required to extract this from MAE features. This is reflected by the strong *linear probe* and  
616 *kNN* performance of DINOv2, while MAE requires *full fine-tuning* to achieve optimal performance.

617 Finally, we note that decoding the desired information from pre-trained features is not always trivial,  
618 and we demonstrate in section 3 that even in the (partially) supervised, fine-tuning setting in GCD,  
619 both of these backbones underperform a randomly initialized ResNet18 on the *count* taxonomy.

## 620 D.5 Understanding cosine classifiers in category discovery

621 Cosine classifiers with entropy regularization have been widely adopted in recognition settings for  
622 which less supervision is available [14, 41], including in category discovery [30, 42]. In fig. 13, we  
623 provide justifications for this by inspecting the norms of the learned vectors in classifiers when these  
624 regularizers are omitted.

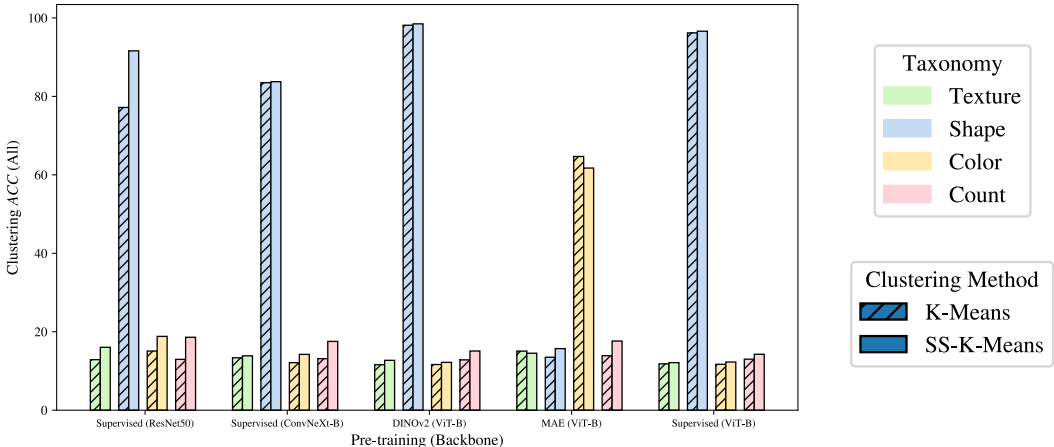


Figure 10: **Effect of semi-supervised  $k$ -means on representative pre-trained backbones.** We find semi-supervised  $k$ -means is insufficient to overcome the bias learned during pre-training.

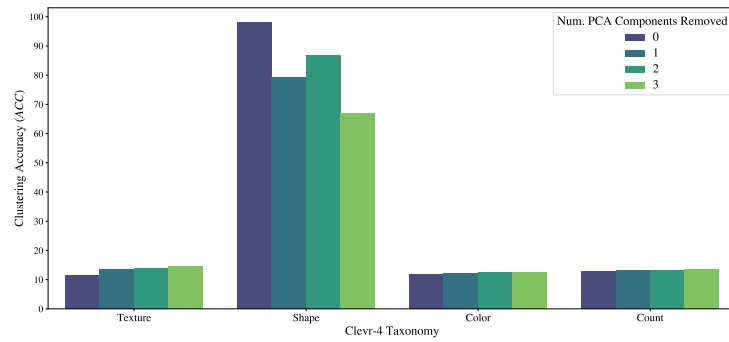


Figure 11: **Re-clustering DINOv2 [29] features after removing dominant principal components.**

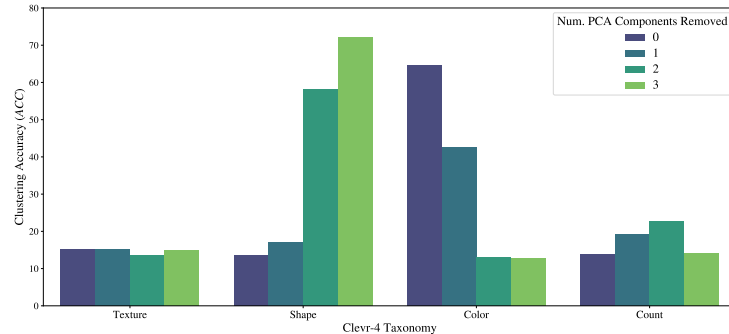


Figure 12: **Re-clustering MAE [26] features after removing dominant principal components.**

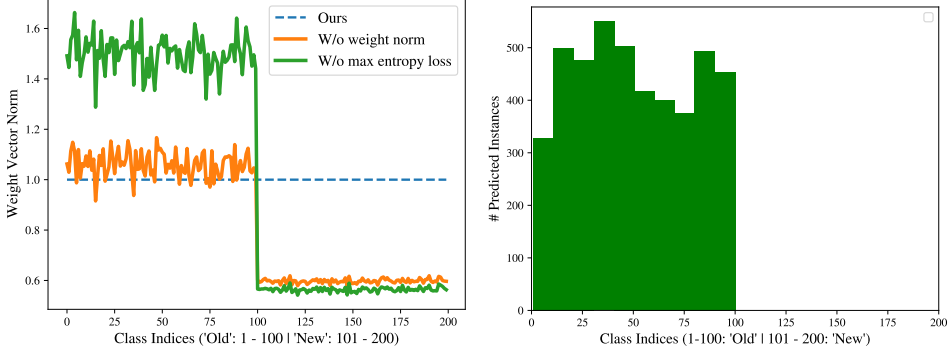


Figure 13: **Left:** Norms of weight vectors in GCD classifiers, with and without regularizations.  
**Right:** Prediction histogram of unregularized classifier.

625 Specifically, consider a classifier (without a bias term) as  $g = \mathbf{W} \in \mathbb{R}^{d \times k}$ , containing  $k$  vectors of  $d$   
 626 dimension, one for each output category. In fig. 13, we plot the magnitude of each of these vectors  
 627 trained with different constraints on CUB [48] (one of the datasets in the SSB [17]). Note that the  
 628 classifier is constructed such that the first 100 vectors correspond to the ‘Old’ classes, and are trained  
 629 with ground truth labels. In our full method, with normalized classifiers, the norm of all vectors is  
 630 enforced to be the unit norm (blue dashed line). If we remove this constraint (solid orange line), we  
 631 can see that the norms of vectors which are *not* supervised by ground truth labels (indices 101-200)  
 632 fall substantially. Then, if we further remove the entropy regularization term (solid green line), the  
 633 magnitudes of the ‘Old’ class vectors (indices 1-200) increases dramatically.

634 This becomes an issue at inference time, with per-class logits computed as:

$$l_m = \langle \mathbf{w}_m, \Phi \rangle = |\mathbf{w}_m| |\Phi| \cos(\alpha) \quad \forall m \in \{1 \dots k\}$$

635 with the class prediction returned as  $\arg \max l_m$ . In other words, we show that without appropriate  
 636 regularisation, our GCD models trivially reduce the weight norm of ‘New’ class vectors  
 637 ( $|\mathbf{w}_m| \quad \forall m > 100$ ), leaving all images to be assigned to one of the ‘Old’ classes. The effects of  
 638 this are visualized in the right panel of fig. 13, which plots the histogram of class predictions for an  
 639 unregularized GCD classifier. We can see that exactly zero examples are predicted to ‘New’ classes.  
 640 We further highlight that this effect is obfuscated by the evaluation process, which reports non-zero  
 641 accuracies for ‘New’ classes through the Hungarian assignment operation.

## 642 D.6 Design of data augmentation and mis-aligned augmentations

643 In our SSB experiments, the teacher is passed a weaker augmentation, comprising only `RandomCrop`  
 644 and `RandomHorizontalFlip`. We find this stabilizes the pseudo-labels produced by the teacher.  
 645 However, the self-supervised literature consistently finds that strong augmentations are beneficial for  
 646 representation learning [9, 14, 24]. As such, we experiment with gradually increasing the strength of  
 647 the augmentation passed to the student model in table 7.

648 Specifically, we experiment along two axes: the strength of the base augmentation (‘Strong Base  
 649 Aug’ column); and how aggressive the cropping augmentation is (‘Aggressive Crop’ column). To  
 650 make the base augmentation stronger, we add Solarization and Gaussian blurring [24]. For cropping,  
 651 we experiment with a light `RandomResizeCrop` (cropping within a range of 0.9 and 1.0) and a  
 652 more aggressive variant (within a range of 0.3 and 1.0). Overall, we find that an aggressive cropping  
 653 strategy, as well as a strong base augmentation, is critical for strong performance. We generally found  
 654 weaker variants to overfit. Though they also have lower peak clustering accuracy, the accuracy falls  
 655 sharply later in training without the regularization from strong augmentation.

656 **Mis-aligned augmentations on Clevr-4** A benefit of Clevr-4 is that each taxonomy has a simple  
 657 semantic axes. As such, we are able to conduct controlled experiments on the effect of targeting these  
 658 axes with different data augmentations. Specifically, in table 8, we demonstrate the effect of having  
 659 ‘misaligned’ augmentations on two splits of Clevr-4. We train the GCD baseline with `ColorJitter`  
 660 on the `color` split and `CutOut` for the `count` split. The augmentations destroy semantic information  
 661 for the respective taxonomies, resulting in substantial degradation of performance. The ‘aligned’

Table 7: Design of student augmentation.

Aggressive Crop	Strong Base Aug	CUB		
		All	Old	New
✗	✗	38.6	54.6	30.6
✗	✓	41.6	58.8	33.0
✓	✗	52.7	<b>69.4</b>	44.7
✓	✓	<b>65.7</b>	68.0	<b>64.6</b>

Table 8: Effect of mis-aligned augmentations on the GCD Baseline.

	Color	Count
Aligned Augmentation	<b>84.5</b>	<b>65.2</b>
Misaligned Augmentation	26.1	46.6

augmentations are light cropping and flipping for *color*, and light rotation for *count*. The results highlight the importance of data augmentation in injecting inductive biases into deep representations.

## D.7 Effect of $\lambda_1$

In fig. 14, we investigate the effect of the hyper-parameter  $\lambda_1$ , which controls the tradeoff between the supervised and unsupervised losses in  $\mu$ GCD. We find that with  $0.1 \leq \lambda_1 \leq 0.4$ , the ‘All’ clustering accuracy is robust, while at  $\lambda_1 = 0$  (only unsupervised loss) and  $\lambda_1 = 1$  (only supervised loss), performance degrades. We note that the Hungarian assignment in evaluation results in imperfect ‘Old’ performance even at  $\lambda_1$  close to 1 (more weight on the supervised loss). As such, we also show an ‘Upper Bound’ (‘cheating’) clustering performance in gray, which allows re-use of clusters in the ‘Old’ and ‘New’ accuracy computation.

## E Additional Experiments

### E.1 Results with estimated number of classes

In the main paper, we followed standard practise in category discovery [7, 30, 42, 46, 47, 57] and *assumed knowledge* of the number of categories in the dataset,  $k$ . Here, we provide experiments when this assumption is removed. Specifically, we train our model using an estimated number of categories in the dataset, where the number of categories is predicted using an off-the-shelf method from [7]. We use estimates of  $k = 231$  for CUB and  $k = 230$  for Stanford Cars, while these datasets have a ground truth number of  $k = 200$  and  $k = 196$  classes respectively.

We compare against figures from SimGCD [30] as well as the GCD baseline [7]. As expected, we find our method performs worse on these datasets when an estimated number of categories is used, though we note that the performance of SimGCD [30] improves somewhat on CUB, and the gap

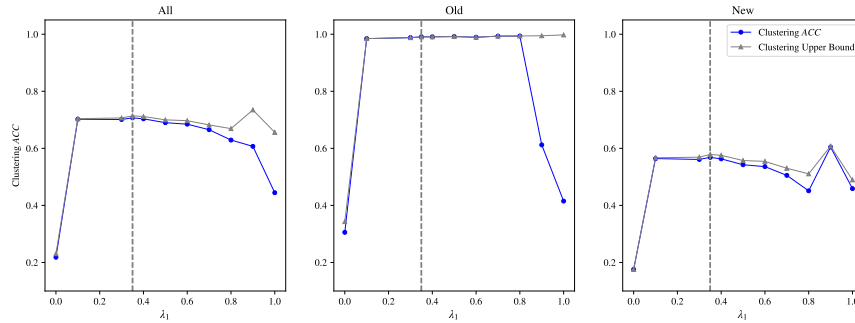


Figure 14: Effect of hyper-parameter,  $\lambda_1$ . We investigate the effect of  $\lambda_1$  (which balances the supervised and un-supervised losses), training  $\mu$ GCD models on the *texture* split.

Table 9: **Results on the SSB with estimated number of categories.** We use the method from [7] to estimate the number of categories as  $k = 231$  for CUB, and  $k = 230$  for Stanford Cars. We run our method with this many vectors in the classification head, comparing against baselines evaluated with the same estimates of  $k$ . Results from baselines are reported from [30].

Pre-training		CUB			Stanford Cars			Average
		All	Old	New	All	Old	New	All
GCD [7]	DINO [14]	47.1	55.1	44.8	35.0	56.0	24.8	41.1
SimGCD [30]	DINO [14]	61.5	<b>66.4</b>	59.1	49.1	65.1	41.3	55.3
$\mu$ GCD (Ours)	DINO [14]	<b>62.0</b>	60.3	<b>62.8</b>	<b>56.3</b>	<b>66.8</b>	<b>51.1</b>	<b>59.2</b>

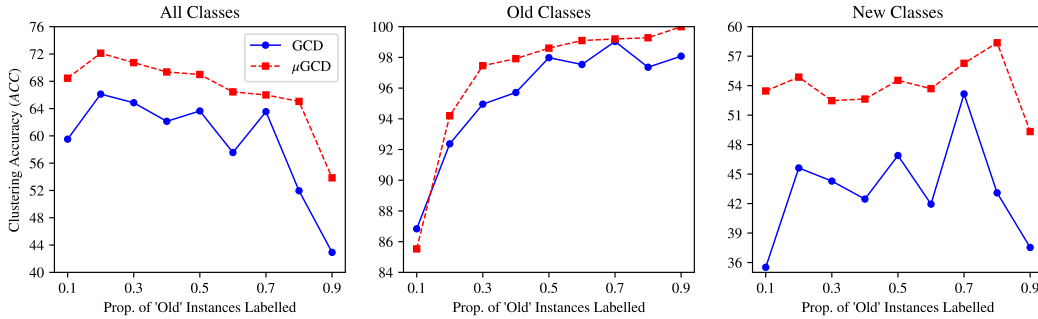


Figure 15: **Results when varying the proportion of ‘Old’ category images reserved for  $\mathcal{D}_L$ .** We find our  $\mu$ GCD method substantially outperforms the GCD baseline [7] across all settings.

683 between our methods is reduced on this dataset. Nonetheless, the proposed  $\mu$ GCD still performs  
684 marginally better on CUB, and further outperforms the SoTA by nearly 7% on Stanford Cars in this  
685 setting.

## 686 E.2 Results with varying proportion of labelled examples

687 In the main paper, we follow standard practise in the GCD setting [7, 30, 46, 47] and sample a fixed  
688 proportion of images,  $p = 0.5$ , from the labelled categories and use them in the labeled set,  $\mathcal{D}_L$ . Here,  
689 we experiment with our method if this proportion changes, showing results in fig. 15. We find our  
690 proposed  $\mu$ GCD substantially outperforms the GCD baseline [7] across all tested values of  $p$ .

## 691 E.3 Results on Herbarium19

692 We evaluate our method on the Herbarium19 dataset [35]. We use the ‘Old’/‘New’ class splits from  
693 [7] which are randomly sampled rather than being curated as they are in the SSB. Nonetheless, the  
694 dataset is highly challenging, being long-tailed and containing 683 classes in total. 341 of these  
695 classes are reserved as ‘Old’, and the dataset contains a total of 34K images. It further contains a  
696 clear taxonomy (herbarium species), making it a suitable evaluation for GCD. We compare  $\mu$ GCD  
697 against prior work in table 10, again finding that we set a new state-of-the-art.

## 698 F Description of baselines and $\mu$ GCD algorithms

699 In this section we provide step-by-step outlines of: the GCD baseline [7]; the SimGCD [30] baseline;  
700 and our method,  $\mu$ GCD. Full motivation of the design decisions in  $\mu$ GCD can be found in section 3.

701 **Task definition and notation:** Given a dataset with labelled ( $\mathcal{D}_L$ ) and unlabelled ( $\mathcal{D}_U$ ) subsets, a  
702 model must classify all images in  $\mathcal{D}_U$  into one of  $k$  possible categories.  $\mathcal{D}_L$  contains only a subset of  
703 the categories in  $\mathcal{D}_U$ , and prior knowledge of  $k$  is assumed. During training, batches ( $\mathcal{B}$ ), are sampled  
704 with both labelled images ( $\mathcal{B}_L \in \mathcal{D}_L$ ) and unlabelled images ( $\mathcal{B}_U \in \mathcal{D}_U$ ). The performance metric is  
705 the clustering (classification) accuracy on  $\mathcal{D}_U$ .

706

707 **GCD [7].** Train a backbone,  $\Phi$ , and perform classification by clustering in its feature space.

Table 10: **Results on Herbarium19** [35], which constitutes a long-tailed GCD evaluation.

Pre-training	Herbarium19			
	All	Old	New	
<i>k</i> -means [23]	DINO [14]	13.0	12.2	13.4
RankStats+ [57]	DINO [14]	27.9	55.8	12.8
UNO+ [42]	DINO [14]	28.3	53.7	12.8
GCD [7]	DINO [14]	35.4	51.0	27.0
ORCA [8]	DINO [14]	20.9	30.9	15.5
OpenCon [46]	DINO [14]	39.3	58.9	28.6
PromptCAL [47]	DINO [14]	37.0	52.0	28.9
MIB [43]	DINO [14]	42.3	56.1	34.8
SimGCD [30]	DINO [14]	43.3	57.9	35.3
$\mu$ GCD (Ours)	DINO [14]	<b>45.8</b>	<b>61.9</b>	<b>37.2</b>

708 (1) Train  $\Phi$  using an unsupervised InfoNCE loss [31] on all the data, as well as a supervised contrastive  
709 loss [32] on the labeled data. Letting  $\mathbf{x}_i$  and  $\mathbf{x}'_i$  represent two augmentations of the same image in a  
710 batch  $\mathcal{B}$ , the unsupervised and supervised losses are defined as:

$$\mathcal{L}_{feat,i}^u = -\log \frac{\exp(\mathbf{z}_i, \mathbf{z}'_i)/\tau}{\sum_{n \neq i} \exp(\mathbf{z}_i, \mathbf{z}_n)/\tau}, \quad \mathcal{L}_{feat,i}^s = -\frac{1}{|\mathcal{N}(i)|} \sum_{q \in \mathcal{N}(i)} \log \frac{\exp(\mathbf{z}_i, \mathbf{z}_q)/\tau}{\sum_{n \neq i} \exp(\mathbf{z}_i, \mathbf{z}_n)/\tau}$$

711 where:  $\mathbf{z}_i = h \circ \Phi(\mathbf{x}_i)$ ;  $h$  is a *projection head*, which is used during training and discarded afterwards;  
712 and  $\tau$  is a temperature value.  $\mathcal{N}(i)$  represents the indices of images in the labeled subset of the  
713 batch,  $\mathcal{B}_L \in \mathcal{B}$ , which belong to the same category as  $\mathbf{x}_i$ . Given a weighting coefficient,  $\lambda_1$ , the total  
714 contrastive loss on the model's features is given as:

$$\mathcal{L}_{feat} = (1 - \lambda_1) \sum_{i \in \mathcal{B}} \mathcal{L}_{feat,i}^u + \lambda_1 \sum_{i \in \mathcal{B}_L} \mathcal{L}_{feat,i}^s \quad (4)$$

715 (2) Perform classification by embedding all images with the trained backbone,  $\Phi$ , and apply semi-  
716 supervised *k*-means (SS-*k*-means) clustering on the entire dataset,  $\mathcal{D}_U \cup \mathcal{D}_L$ . SS-*k*-means is identical  
717 to unsupervised *k*-means [23] but, at each iteration, instances from  $\mathcal{D}_L$  are always assigned to the  
718 ‘correct’ cluster using their labels, before being used in the centroid update. In this way, the cluster  
719 centroid updates for labelled classes are guided by the labels in  $\mathcal{D}_L$ .

720 **SimGCD [30].** Train a backbone representation,  $\Phi$ , and a linear head,  $g$ , to classify images amongst  
721 the  $k$  classes in the dataset, yielding a model  $f_\theta = g \circ \Phi$ . Train the backbone *jointly* with the feature  
722 space loss from eq. (4), and with linear classification losses based on the output of  $g$ .

723 (1) Generate *pseudo-labels* for an image,  $\mathbf{x}_i$ , as  $\mathbf{p}_T(\mathbf{x}_i) \in [0, 1]^k$ , in order to train the classifier,  $f_\theta$ .  
724 Infer pseudo-labels on all images in a batch,  $\mathcal{B}$ , and compute an additional supervised cross-entropy  
725 loss on the labelled subset,  $\mathcal{B}_L$ .

- 726 • Pass two views of an image to the *same model*. Each view generates a soft pseudo-label for  
727 the other, for instance as:

$$\mathbf{p}_T(\mathbf{x}_i) = \text{sg}[\text{softmax}(f_\theta(\mathbf{x}'_i); \tau_T)] \quad (5)$$

728 Here sg is the stop-grad operator and  $\tau_T$  is the pseudo-label temperature.

- 729 • Compute model predictions as  $\mathbf{p}_S(\mathbf{x}) = \text{softmax}(f_\theta(\mathbf{x}); \tau_S)$  and a standard pseudo-  
730 labelling loss [14, 18, 38] (*i.e.* soft cross-entropy loss) as:

$$\mathcal{L}_{cls}^u(\theta; \mathcal{B}) = -\frac{1}{|\mathcal{B}|} \sum_{\mathbf{x}_i \in \mathcal{B}} \langle \mathbf{p}_T(\mathbf{x}_i), \log(\mathbf{p}_S(\mathbf{x}_i)) \rangle + \langle \mathbf{p}_T(\mathbf{x}'_i), \log(\mathbf{p}_S(\mathbf{x}'_i)) \rangle \quad (6)$$

731 Temperatures are chosen such that  $\tau_T < \tau_S$  to encourage confident pseudo-labels [14].

- 732 • Optimize the model,  $f_\theta$ , *jointly* with: the pseudo-label loss (eq. (6)) and  $\mathcal{L}_{feat}$  (see eq. (4)).  
733 The model is further trained with: the standard supervised cross-entropy loss on the labelled  
734 subset of the batch,  $\mathcal{L}_{cls}^s(\theta; \mathcal{B}_L)$ ; and an entropy regularization term,  $\mathcal{L}_{cls}^r(\theta)$ :

$$\mathcal{L}_{cls}^s(\theta; \mathcal{B}_L) = -\frac{1}{|\mathcal{B}_L|} \sum_{i \in \mathcal{B}_L} \langle \mathbf{y}(\mathbf{x}), \log(\mathbf{p}_S(\mathbf{x})) \rangle, \quad \mathcal{L}_{cls}^r(\theta) = -\langle \bar{\mathbf{p}}_S, \log(\bar{\mathbf{p}}_S) \rangle, \quad \bar{\mathbf{p}}_S = \frac{1}{|\mathcal{B}|} \sum_{\mathbf{x} \in \mathcal{B}} \mathbf{p}_S(\mathbf{x})$$

735 Here,  $\mathbf{y}(\mathbf{x})$  is a ground-truth label and, given hyper-parameters  $\lambda_1$  and  $\lambda_2$ , the total loss is defined as:  
 736  $\mathcal{L}(\theta; \mathcal{B}) = (1 - \lambda_1)(\mathcal{L}_{cls}^u(\theta; \mathcal{B}) + \mathcal{L}_{feat}^u(\theta; \mathcal{B})) + \lambda_1(\mathcal{L}_{cls}^s(\theta; \mathcal{B}_L) + \mathcal{L}_{feat}^s(\theta; \mathcal{B}_L)) + \lambda_2 \mathcal{L}_{cls}^r(\theta)$ .

737

738  **$\mu$ GCD (Ours).** Train a backbone representation,  $\Phi$ , and a linear head,  $g$ , to classify images amongst  
 739 the  $k$  classes in the dataset, yielding a model  $f_{\theta_T} = g \circ \Phi$ . Train the backbone *first* with the feature  
 740 space loss from eq. (4), and *then* with linear classification losses based on the output of  $g$ .

741 (1) Train a backbone  $\Phi$  using Step (1) from the GCD baseline algorithm.

742 (2) Append a classifier,  $g$ , to the backbone and duplicate it to yield two models. One model (a *teacher*  
 743 *network*,  $f_{\theta_T}$ ) is used to generate pseudo-labels for a *student network*,  $f_{\theta_S}$ , as  $\mathbf{p}_T(\mathbf{x}_i) \in [0, 1]^k$ . Infer  
 744 pseudo-labels on all images in a batch,  $\mathcal{B}$ , and compute an additional supervised cross-entropy loss  
 745 on the labelled subset,  $\mathcal{B}_L$ . The student and teacher networks are trained as follows:

- 746 • Generate a *strong augmentation* of an image,  $\mathbf{x}_i$ , and a *weak augmentation*,  $\mathbf{x}'_i$  [39]. Pass  
 747 the weak augmentation to the *teacher* to generate a pseudo-label and construct a loss:

$$\mathbf{p}_T(\mathbf{x}_i) = \text{sg}[\text{softmax}(f_{\theta_T}(\mathbf{x}'_i); \tau_T)] \quad \mathcal{L}_{cls}^u(\theta_S; \mathcal{B}) = -\frac{1}{|\mathcal{B}|} \sum_{\mathbf{x}_i \in \mathcal{B}} \langle \mathbf{p}_T(\mathbf{x}_i), \log(\mathbf{p}_S(\mathbf{x}_i)) \rangle \quad (7)$$

- 748 • Optimize the student’s parameters,  $\theta_S$ , with respect to: the pseudo-label loss from eq. (7);  
 749 the supervised loss,  $\mathcal{L}_{cls}^s$ ; and the entropy regularization loss,  $\mathcal{L}_{cls}^r$ . Formally, the ‘student’,  
 750  $f_{\theta_S}$ , is optimized for:  $\mathcal{L}(\theta_S; \mathcal{B}) = (1 - \lambda_1)\mathcal{L}_{cls}^u(\theta_S; \mathcal{B}) + \lambda_1\mathcal{L}_{cls}^s(\theta_S; \mathcal{B}_L) + \lambda_2\mathcal{L}_{cls}^r(\theta_S)$ .  
 751 • Update the teacher network’s parameters with the Exponential Moving Average (EMA) of  
 752 the student network [36]. Specifically, update the ‘teacher’ parameters,  $\theta_T$ , as:

$$\theta_T = \omega(t)\theta_T + (1 - \omega(t))\theta_S$$

753 where  $t$  is the current epoch and  $\omega(t)$  is a time-varying decay schedule.

754 At the end of training, the ‘teacher’,  $f_{\theta_T}$ , is used for evaluation.

755 **Remarks:** We first highlight the different ways in which the labels from  $\mathcal{D}_L$  are used between the  
 756 three methods. Specifically, the GCD baseline [7] only uses the labels in a feature-space supervised  
 757 contrastive loss. However, in addition to this, SimGCD [30] and  $\mu$ GCD *also* use the labels in a  
 758 standard cross-entropy loss in order to train part of a linear classifier,  $g$ .

759 We further note the high level similarity between SimGCD and  $\mu$ GCD, in that both train parametric  
 760 classifiers with a pseudo-label loss. While SimGCD uses different views passed to the same model  
 761 to generate pseudo-labels for each other (similarly to SWaV [9]),  $\mu$ GCD uses pseudo-labels from a  
 762 ‘teacher’ network to train a ‘student’ (similarly to mean-teachers [36]).

763 This is in keeping with trends in related fields, which find that there exists a small kernel of method-  
 764 ologies — *e.g.*, mean-teachers [36], cosine classifiers [40], entropy regularization [18] — which are  
 765 robust across many tasks [14, 27, 41], but that *finding a strong recipe* for a specific problem is critical.  
 766 We find this to be true in supervised classification [25, 58, 59], self-supervised learning [14, 24], and  
 767 semi-supervised learning [18, 36, 39]. Our use of mean-teachers to provide classifier pseudo-labels,  
 768 as well as careful choice of model initialization and data augmentation, yields a performant  $\mu$ GCD  
 769 algorithm for category discovery.

## 770 G Further Implementation Details

771 When re-implementing prior work, we aim to follow the hyper-parameters of the GCD baseline [7]  
 772 and SimGCD [30], and use the same settings for our method. We occasionally find that tuned  
 773 hyper-parameters are beneficial in some settings, which we detail below.

774 **Learning rates.** We swept learning rates at factors of 10 for all methods and architectures. When  
775 training models from scratch (ResNet18 on Clevr-4) or when finetuning a DINO/DINOv2 model [14,  
776 29] on the SSB, we found a learning rate of 0.1 to be optimal. When finetuning an MAE [26] or  
777 DINOv2 model on Clevr-4, we found it better to lower the learning rate to 0.01. All learning rates are  
778 decayed from their initial value by a factor of  $10^{-3}$  throughout training with a cosine schedule.

779 **Loss hyper-parameters.** For the tradeoff between the unsupervised and supervised components of  
780 the losses,  $\lambda_1$  is set to 0.35 for all methods. For the entropy regularization, we follow SimGCD and  
781 use  $\lambda_2 = 1.0$  for FGVC-Aircraft and Stanford Cars, and  $\lambda_2 = 2.0$  for all other datasets. We swept  
782 to find better settings for this term on Clevr-4, but did not find any setting to consistently improve  
783 results. We also train with  $L^2$  weight decay, set to  $10e^{-4}$  for all models.

784 **Student and teacher temperatures.** Following [14], we set the temperature of the student and  
785 teacher to  $\tau_S = 0.1$  and  $\tau_T = 0.04$  respectively, for both our method and SimGCD. This gives  
786 the teacher ‘sharper’ (more confident) predictions than the student. We further follow the teacher-  
787 temperature warmup schedule from [14], also used in SimGCD, where the teacher temperature is  
788 decreased from 0.07 to 0.04 in the first 30 epochs of training. On Herbarium19 [35] (which has  
789 many more categories than the other evaluations, see appendix E.3), we use a teacher temperature of  
790  $2 \times 10^{-3}$  (warmed up from  $3.5 \times 10^{-3}$  over 10 epochs).

791 **Teacher Momentum Schedule.** In  $\mu$ GCD, at each iteration, the teacher’s parameters are linearly  
792 interpolated between the teacher’s current parameters and the student’s, with the interpolation (‘decay’)  
793 or ‘momentum’) changing over time following [38], as:  $\omega(t) = \omega_T - (1 - \omega_{base})(\cos(\frac{\pi t}{T}) + 1)/2$ .

794 Here  $T$  is the total number of epochs and  $t$  is the current epoch. We use  $\omega_T = 0.999 \approx 1$  and  
795  $\omega_{base} = 0.7$ . We note for clarity that, though the momentum parameter is dictated by the *epoch*  
796 number, the teacher update happens at each *gradient step*.

797 **Augmentations.** On Clevr-4 we use an augmentation comprising of RandomHorizontalFlip  
798 and RandomRotation. On the SSB [17], we use RandomHorizontalFlip and  
799 RandomCrop. We use these augmentations for all methods, and for  $\mu$ GCD use these augmentations  
800 to pass views to the ‘teacher’. An important part of our method on the SSB is to design **strong**  
801 augmentations to pass to the student. Our ‘strong augmentation’ adds aggressive RandomResizeCrop,  
802 as well as solarization and Gaussian blurring [24] (see appendix D.6 for details). On Clevr-4, due  
803 to the relatively simple nature of the images, strong augmentations can destroy the semantic image  
804 content; for instance color jitter and aggressive cropping degrade performance on *color* and *count*  
805 respectively. We find it helpful to pass Cutout [60] to the teacher on the *color* taxonomy, and *texture*  
806 benefits from the strong augmentation defined above.

807 **Training time.** Following the original implementations, we train all SimGCD [30] and GCD base-  
808 line [7] models for 200 epochs, which we find sufficient for the losses (and validation performance)  
809 to plateau. For our method, we randomly initialize a classifier on a model which has been trained  
810 with the GCD baseline loss, and further finetune for another 100 epochs. On our hardware (either an  
811 NVIDIA P40 or M40) we found training to take roughly 15 hours for SSB datasets, and around 4  
812 hours for a Clevr-4 experiment.

813 **Early stopping.** We note that GCD is a *transductive* setting, or a *clustering* problem, where models  
814 are trained (in an unsupervised fashion) on the data used for evaluation,  $\mathcal{D}_{\mathcal{U}}$ . As such, an important  
815 criterion is *which metric* to use to select the best model. SimGCD [30] and the GCD baseline [7] use  
816 the performance on a validation set of images from the labeled categories. While this is a reasonable  
817 choice for the baseline, we found it can lead to underestimated performance for SimGCD on some  
818 datasets. For SimGCD, we instead found it better to simply take the model at the end of training.  
819 For  $\mu$ GCD, we instead propose to choose the model with the minimum *unsupervised loss* on the  
820 unlabeled set.

821 **Other details:** When finetuning pre-trained transformer models – DINO [14], DINOv2 [29] or  
822 MAE [26] – we finetune the last transformer block of the model. For Clevr-4, when training a  
823 ResNet18, we finetune the whole model. Finally, for the  $\mu$ GCD failure case of *shape*, we suggest  
824 in appendix D.2 that  $\mu$ GCD can get stuck in local optima if its initialization is already very strong.  
825 As such, in this case, we initialize the linear head with  $k$ -means centroids, reduce the learning rate  
826 and teacher temperature to 0.01, and set  $\omega_{base}$  to 0.9.

827 **H Related Work**

828 **Representation learning.** The common goal of self-, semi- and unsupervised learning is to learn  
829 representations with minimal labelled data. A popular technique is contrastive learning [24, 27],  
830 which encourages representations of different augmentations of the same training sample to be similar.  
831 Contrastive methods are typically either based on: InfoNCE [31] (*e.g.*, MoCo [37] and SimCLR [24]);  
832 or online pseudo-labelling (*e.g.*, SWaV [9] and DINO [14]). Almost all contrastive learning methods  
833 now adopt a variant of these techniques [18, 41, 61, 62]. Another important component in many  
834 pseudo-labelling based methods is ‘mean-teachers’ [36] (or momentum encoders [37]), in which a  
835 ‘teacher’ network providing pseudo-labels is maintained as the moving average of a ‘student’ model.  
836 Other learning methods include cross-stitch [63], context-prediction [64], and reconstruction [26]. In  
837 this work, we use mean-teachers to build a strong recipe for GCD.

838 **Attribute learning.** We propose a new synthetic dataset which contains multiple taxonomies based  
839 on various attributes. Attribute learning has a long history in computer vision, including real-world  
840 datasets such as the Visual Genome [65], with millions of attribute annotations, and VAW, with  
841 600 attributes types [66]. Furthermore, the *disentanglement literature* [67–69] often uses synthetic  
842 attribute datasets for investigation [70, 71]. We find it necessary to develop a new dataset, Clevr-  
843 4, for category discovery as real-world datasets have either: noisy/incomplete attributes for each  
844 image [65, 72]; or contain sensitive information (*e.g.* contain faces) [73]. We find existing synthetic  
845 datasets unsuitable as they do not have enough categorical attributes which represent ‘semantic’  
846 factors, with attributes often describing continuous ‘nuisance’ factors such as object location or  
847 camera pose [70, 71, 74].

848 **Category Discovery.** Novel Category Discovery (NCD) was initially formalized in [20]. It differs  
849 from GCD as the unlabelled images are known to be drawn from a *disjoint* set of categories to the  
850 labelled ones [42, 44, 57, 75, 76]. This is different from *unsupervised clustering* [10, 77], which  
851 clusters unlabelled data without reference to labels at all. It is also distinct from *semi-supervised*  
852 *learning* [18, 36, 39], where unlabelled images come from the *same* set of categories as the labelled  
853 data. GCD [7, 8] was recently proposed as a challenging task in which assumptions about the classes  
854 in the unlabelled data are largely removed: images in the unlabelled data may belong to the labelled  
855 classes or to new ones [30, 43, 46, 47]. We particularly highlight concurrent work in SimGCD [30],  
856 which reports the best current performance on standard GCD benchmarks. Our method differs from  
857 SimGCD by the adoption of a mean-teacher [36] to provide more stable pseudo-labels training,  
858 and by careful consideration of model initialization and data augmentations. [46] also adopt a  
859 momentum-encoder, though only for a set of class prototypes rather than in a mean-teacher setup.

860 **H.1 Clevr-4: connections to real-world and disentanglement datasets**

861 **Datasets with different granularities.** When multiple taxonomies are defined in existing datasets,  
862 they are most often specified only at different *granularities*, for instance in CIFAR100 [19], FGVC-  
863 Aircraft [22] and iNaturalist [78]. While recognition at different granularities is related to our task –  
864 and was explored in [79] – the constituent taxonomies are not *statistically independent*, as the Clevr-4  
865 splits are. We note that, given the number of categories in each taxonomy, an unsupervised model  
866 could in principle solve the clustering problem at the different granularities.

867 **CUB-200-2011 [48].** Fei *et al.* [45] discuss the existence of alternate, but valid, clusterings of images  
868 from fine-grained datasets like CUB [48] – *e.g.*, based on pose or background. We note that the CUB  
869 ‘Birds’ dataset presents an opportunity for constructing an interesting dataset for category discovery.  
870 Each image in CUB is labelled for presence (or absence) of each of 312 attributes, where these  
871 attributes come from different *attribute types*. Each attribute type (*e.g.*, ‘bill shape’, ‘breast color’)  
872 provides a different taxonomy with respect to which to cluster the data. However, we found these  
873 attribute annotations are too noisy to yield meaningful conclusions.

874 **Disentanglement datasets.** We suggest that Clevr-4 is also a useful benchmark for disentanglement  
875 research [67, 68]. This research field aims to learn models such that the ground-truth data generating  
876 factors (*i.e.*, attributes of an object) are encoded in different subspaces of the image representation.  
877 The current CLEVR dataset [12] cannot be used easily for this, as its images contain multiple objects,  
878 each with different attributes. Instead, in Clevr-4, all objects share the same attributes, allowing each  
879 image to be fully parameterized by the object *shape*, *texture*, *color* and *count*. Furthermore, compared  
880 to synthetic datasets for disentanglement [71], Clevr-4 contains more categorical taxonomies, as well  
881 as more classes within those taxonomies.

882 Finally, we note that there exist other extensions of the CLEVR dataset [12], such as ClevrTex [80],  
883 Super-CLEVR [81] and CLEVR-X [82], which also add new textures and/or categories to the original  
884 datasets. However these datasets *cannot* be used for category discovery (or disentanglement) research  
885 as, unlike in Clevr-4, they contain scenes with objects of differing attributes. As such, each image  
886 cannot be parameterized with respect to the object attributes in a way which gives rise to clear  
887 taxonomies.

888 **Other related fields** The GCD task and the Clevr-4 dataset are related to a number of other machine  
889 learning sub-fields. *Conditional Similarity* research [83–85] aims to learn different embedding  
890 functions given different *conditions*. For instance, the GeneCIS benchmark [83] evaluates the  
891 ability of models to retrieve different images given a query and different conditioning text prompt.  
892 Meanwhile, the *multiple clustering* [86, 87] and *self-supervised learning* [88, 89] fields investigate  
893 the how different choices of data augmentation result in different clusterings of the data. The  
894 self-supervised field particularly aims to understand why these inductive biases result in different  
895 generalization properties [90–92].

896 We hope that Clevr-4 can be complementary to these works, and provide a test-bed for controlled  
897 experimentation of these research questions.

898 **H.2  $\mu$ GCD method.**

899 We note here that the idea of momentum encoders has been widely used in representation learning [37,  
900 38, 47], semi-supervised learning [36, 41], or to update class prototypes in category discovery [46, 93].  
901 We use a mean-teacher model *end-to-end*, for the backbone representation and the classification head.  
902 We highlight that, similar to a rich vein of literature in related fields [14, 18, 24, 25, 58, 59], our goal  
903 is to find a specific recipe for the GCD task.